1958

Stress distribution in ship bulkheads with various stiffening and bottom support: a photoelastic study

Norman, Thomas Victor.; Rodriguez Guiterrez, Gerardo Augusto.
Massachusetts Institute of Technology

http://hdl.handle.net/10945/26792

STRESS DISTRIBUTION IN SHIP BULKHEADS WITH VARIOUS STIFFENING AND BOTTOM SUPPORT

A PHOTOELASTIC STUDY

THOMAS VICTOR NORMAN, JR.
AND
GERARDO AUGUSTO RODRIGUEZ GUTIERREZ

STRESS DISTRIBUTION IN SHIP BULKHEADS WITH VARIOUS STIFFENING AND BOTTOM SUPPORT
A PHOTOELASTIC STUDY

by

THOMAS VICTOR NORMAN, JR.

and

GERARDO AUGUSTO RODRIGUEZ GUTIERREZ

SUBMITTED IN PARTIAL FULFILLMENT OF THE

REQUIREMENTS FOR THE DEGREE OF NAVAL ENGINEER

and

FOR THE DEGREE OF MASTER OF SCIENCE IN

NAVAL ARCHITECTURE AND MARINE ENGINEERING

at the

MASSACHUSETTS INSTITUTE OF TECHNOLOGY

MAY, 1958

STRESS DISTRIBUTION IN SHIP BULKHEADS WITH VARIOUS STIFFENING AND BOTTOM SUPPORT -

A PHOTOELASTIC STUDY

by

THOMAS VICTOR NORMAN, JR.

and

GERARDO AUGUSTO RODRIGUEZ GUTIERREZ

Submitted to the Department of Naval Architecture and Marine Engineering on May 26, 1958 in partial fulfillment of the requirements for the degree of Naval Engineer and for the degree of Master of Science in Naval Architecture and Marine Engineering.

ABSTRACT

This thesis is a continuation of the work started by E. A. Miller and J. T. Metcalf (reference 1). It is also part of the large field of work covered in references 2, 3 and 4. The general objective of the field is the collection and analysis of data to be used to improve the design of ship transverse bulkheads. This thesis completed the work started in reference 1, by determining the shear stress distribution along clamped edges of plates of aspect ratios 1:1, 2:1, 3:1 and 5:1 with 0, 1, 2 and 3 stiffeners under a uniformly distributed top edge loading and with the bottom either unsupported or supported.

As with the previous work in the field, the photoelastic technique was employed. The plots of this distribution are shown in the section of results and are non-dimensional in character. The results of reference 1 are incorporated in this thesis for comparison and summation. In general the results of the two thesis agree closely.

It is recommended that further work in the field be directed toward the determination of the percentage of bottom support that is present in the actual ship bulkhead.

Thesis Supervisor: Dr. W. M. Murray

Title: Professor of Mechanical Engineering

ACKNOWLEDGEMENT

The authors wish to express their appreciation to:

Dr. William M. Murray, of the Department of Mechanical Engineering, who acted as thesis supervisor and who assisted us greatly in the field of photoelastic techniques.

Professor J. Harvey Evans, of the Department of Naval Architecture and Marine Engineering, who directed us in the field of ship bulkhead research, and permitted us to use the ship's structure laboratory and equipment therein.

Mr. Jerome Catz, of the Department of Mechanical Engineering, for his technical advice and assistance with the equipment of the Stress Analysis Laboratory.

Cambridge 39, Massachusetts
May 26, 1958

Secretary of the Faculty
Massachusetts Institute of Technology
Cambridge 39, Massachusetts

Dear Sir:

In accordance with the requirements for the degree of Naval Engineer and for the degree of Master of Science in Naval Architecture and Marine Engineering, we herewith submit a thesis entitled, "Stress Distribution in Ship Bulkheads with Various Stiffening and Bottom Support - A Photoelastic Study."

Respectfully submitted,

TABLE OF CONTENTS

TABLE OF ILLUSTRATIONS

TABLES OF DATA

ABBREVIATIONS

σ_1, σ_2	Principal stresses (pounds per square inch)
σ_x, σ_y	Stresses in x- and y-directions (pounds per square inch)
τ_{max}	Maximum shear stress at any point (pounds per square inch)
τ_m	Average shear stress over the boundary (pounds per square inch)
τ_{xy}	Shear stress in the plane perpendicular to the axis, and in the y direction (pounds per square inch)
f	Fringe constant of the material (pounds per inch per order)
h	Thickness of the model
n	Order of interference
θ	Direction of principal stresses from the x-and y-axes clockwise (degrees)
b	Depth of model in y-direction (inches)
l	Distance between model supports (inches)
M	Bending moment (pound inches)
y	Distance from neutral axis to any point on the model (inches)
I	Moment of inertia of cross section (inches^4)
AR	Aspect ratio (inches per inch)
w	Uniform load (pound per inch)
Δ	Small increment of following element

I. INTRODUCTION

In the design of ships' bulkheads the engineer attempts to use the minimum weight that is consistent with the necessary strength for supporting the load. The usual procedure is to design the bulkhead to withstand the hydrostatic load that would be imposed if the adjoining compartment were flooded to the waterline. However, the bulkhead must, prior to damage and flooding, transmit its share of the load from the upper boundary into the framework of the ship. In some cases this is more important than the hydrostatic load which would be applied.

This vertical load imposed along the top edge may either be transmitted to the side shell of the ship or directly into the bottom. This is the nebulous phase of the design procedure. The rigidity of the connections to the side and the rigidity of the bottom connections are always in serious doubt. If, for the present, it is assumed that the side connections are perfectly rigid, as in an ideal cantilever, then the rigidity of the bottom is the governing factor. There are two possible extremes, either the bottom is completely unyielding or it is completely free to move. Since there are valid arguments against each case, the actual condition must lie in the region between these extremes.

The next question concerning this transmission of load lies in the problem of the shear load at the shell. The shear stress along this boundary governs the size of the plating that will sustain the load. When looking for a minimum weight solution it is desirable to use only that thickness of plating required, and

here the stress distribution along the edge has to be known.

This is the object of this thesis, to give experimental data so that the stress distribution along the shell may be better known. The current Bureau of Ships practice is to assume, in the absence of an intervening deck, that only the top seven (7) feet are useful in this transmission of sheer stress to the shell. This selection seems to be too arbitrary in view of the loading on bulkheads of various sizes and shapes. References (1), (2), (3), and (4) show that these bulkheads fall in the range between deep beams and flat plates and that any theoretical solution to the problem is tremendously complicated.

References (2), (3), and (4) studied this problem with the assumption of concentrated loads along the top edge, and reference (1) investigated the effects of uniformly distributed loading. This thesis continues the work of reference (1) and completes all tests on models of aspect ratios 1:1, 2:1, 3:1, and 5:1 with up to three symmetric stiffeners. Both cases, bottom edge completely unsupported and bottom edge rigidly supported, were investigated in order to establish the extremes that would be expected. Results are given in dimensionless system of units, τ_{xy}/τ_m , to permit ease in extrapolation from model to full-scale structure.

The use of photoelasticity has proved to be a successful and easy method of determining stress distribution in two-dimensional problems, by means of models which are easy to construct and study. It is especially adaptable to both beam study and flat-plate study and, therefore, is very important in this investigation.

With the results of references (1), (2), (3), and (4) and this thesis there are two more aspects of the problem left for further study. First, the true loading on the top edge, either uniformly distributed or concentrated, or some combination of these; and second, the per cent of rigidity of bottom support that is present.

II PROCEDURE

To accomplish the goal of calculating the stress distribution along the clamped edges of a flat plate under edge loading, the photoelastic technique was employed. In reference (5) the formula for the difference in principal stresses was shown to be

$$\sigma_x - \sigma_y = \frac{f\ n}{h}\ ; \quad \text{where } f = \text{fringe constant of the material}$$
$$n = \text{order of interference}$$
$$h = \text{thickness of model}$$

From strength of materials, it is known that the shear stress at any point can be calculated from the formula

$$\tau_{xy} = \frac{\sigma_x - \sigma_y}{2} \sin 2\theta$$

where θ = the angular displacement of the principal stresses from the axis of the desired shear stress. Combining the two formulae, we obtain

$$\tau_{xy} = \frac{f\ n}{2\ h} \sin 2\theta$$

The quantities in the above equation are obtainable by using photoelastic procedures, and therefore the stress at any point can be calculated.

Two types of materials were used in the models for this thesis. To determine the order of interference, models made of Catalin were used and models of Plexiglas were made to determine the angle of principal stress orientation to the vertical direction.

In all cases the models were rigidly supported at both ends, and uniformly loaded across the top edge by means of a special loading device described in Appendix A. The orders of interference were determined for the Catalin models at eleven

points along the edge by using mercury vapor light and a standard polariscope. A photograph was taken of each model at the testing load and these are included in Appendix E. The angles of principal stresses were obtained for each model for each of these eleven points by using white light and a plane polariscope, with Plexiglas models. Sketches of the isoclinic lines for each model tested appear also in Appendix E.

The following models were included in the series of tests:

AR	Number of stiffeners
1:1	0
1:1	1
1:1	2
1:1	3
2:1	2
2:1	3
3:1	2
5:1	2
5:1	3

Each model was tested, both with the bottom edge completely unsupported and with the bottom edge rigidly supported. Altogether there were eighteen (18) tests conducted to obtain orders of interference, and eighteen (18) tests were conducted to determine the values of stress direction (θ).

As we have stated before, the shear stress at each point can be calculated if these two values for each point along the ends are known and the fringe constant for the material (see Appendix C) has been obtained. This value was compared with the mean shear stress value obtained from the formula

$$\tau_m = \frac{w \times 1}{2 \times h \times b}$$

where w = uniform load across the top edge in lb /in (Appendix D)

l = length of top edge, inches

h = thickness of model, inches

b = width of model, inches

The dimensionless ratio τ_{xy}/τ_m was then plotted for each point along the edge for each of the eighteen (18) models tested.

III-RESULTS

The results of this thesis are shown by the stress distributions along a clamped edge of the models indicated in the following figures:

Figure I shows the distribution for the four stiffening arrangements of aspect ratio 1:1 without bottom support.

Figure II shows the distribution for the four stiffening arrangements of aspect ratio 1:1 with bottom support.

Figure III shows the distribution for the four stiffening arrangements of aspect ratio 2:1 without bottom support. The distribution curves for 0 stiffener and 1 stiffener were obtained from reference (1).

Figure IV shows the distribution for the four stiffening arrangements of aspect ratio 2:1 with bottom support. The distribution curves for 0 stiffener and 1 stiffener were obtained from reference (1).

Figure V shows the distribution for the four stiffening arrangements of aspect ratio 3:1 without bottom support. The distribution curves for 0, 1, and 3 stiffeners were obtained from reference (1).

Figure VI shows the distribution for the four stiffening arrangements of aspect ratio 3:1 with bottom support. The distribution curves for 0, 1, and 3 stiffeners were obtained from reference (1).

Figure VII shows the distribution for the four stiffening arrangements of aspect ratio 5:1 without bottom

support. The distribution curves for 0 and 1 stiffeners were obtained from reference (1).

Figure VIII shows the distribution for the four stiffening arrangements of aspect ratio 5:1 with bottom support. The distribution curves for 0 and 1 stiffeners were obtained from reference (1).

Figure I

Plot of τ_{xy}/τ_m for AR 1:1 for four degrees of stiffening and unsupported

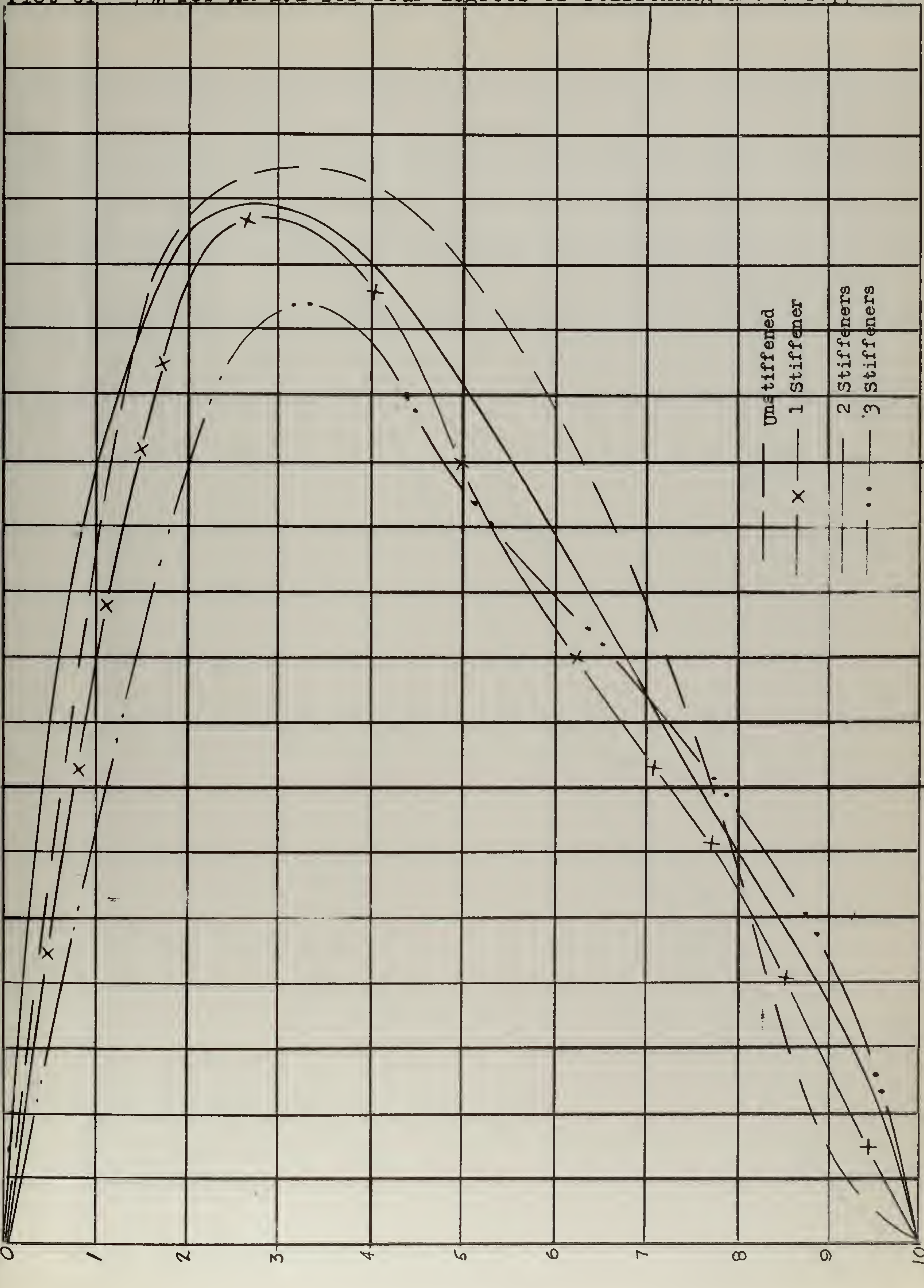

Figure II

Plot of τ_{xy}/τ_m for AR 1:1 for four degrees of stiffening and supported

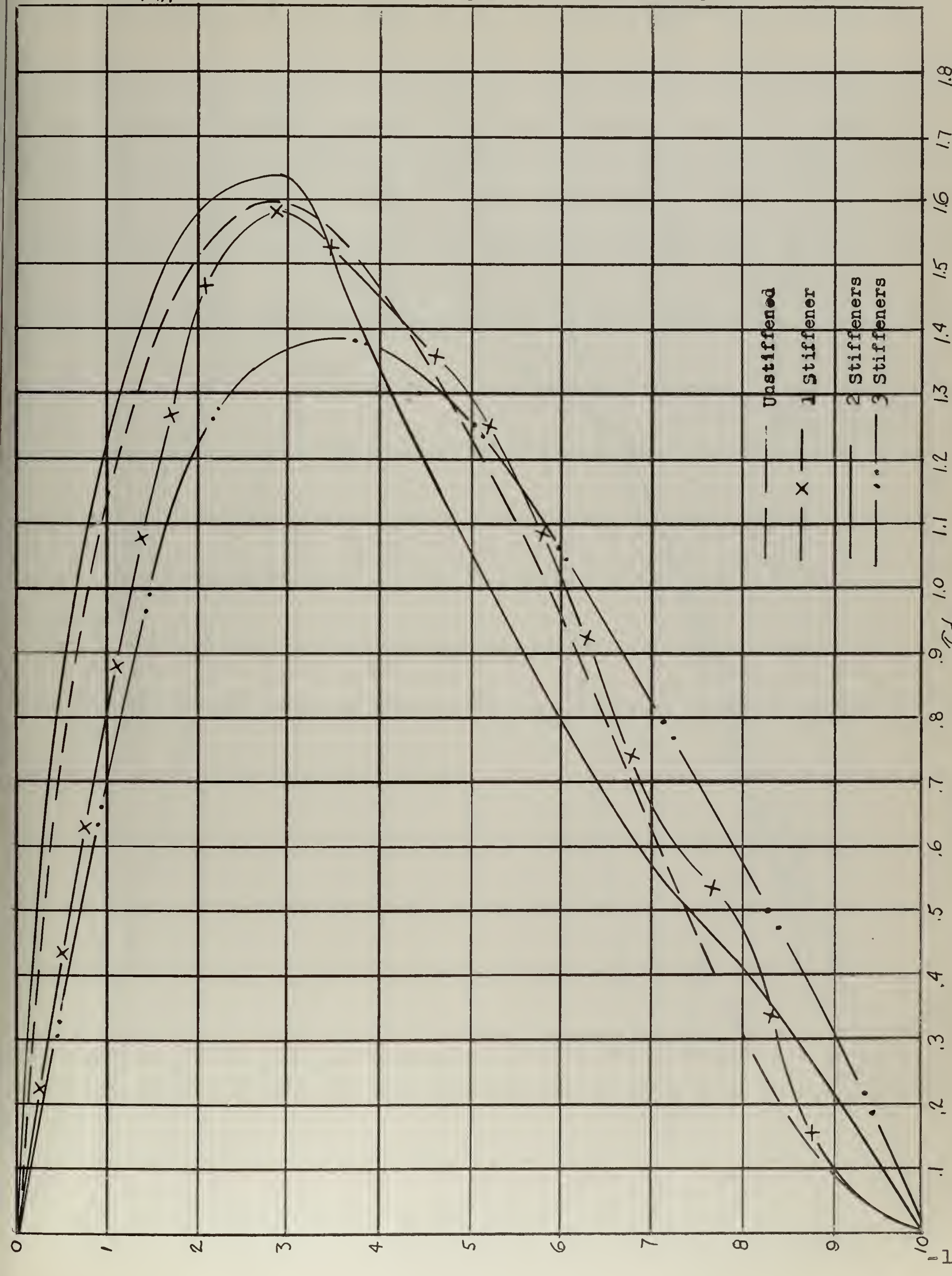

Figure III

Plot of τ_{xy}/τ_m for AR 2:1 for four degrees of stiffening and unsupported

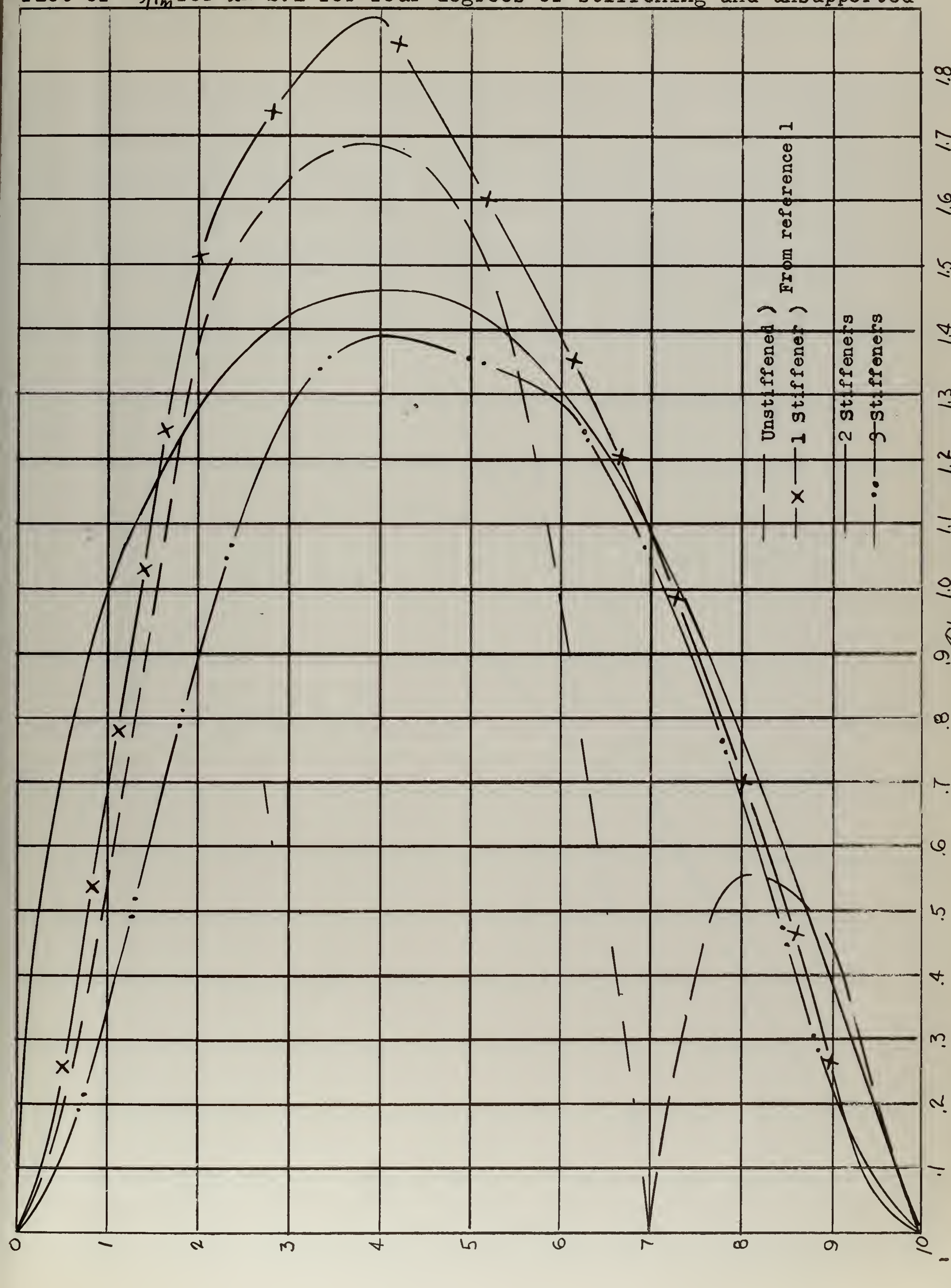

Figure IV

Plot of τ_{xy}/τ_m for AR 2:1 for four degrees of stiffening and supported

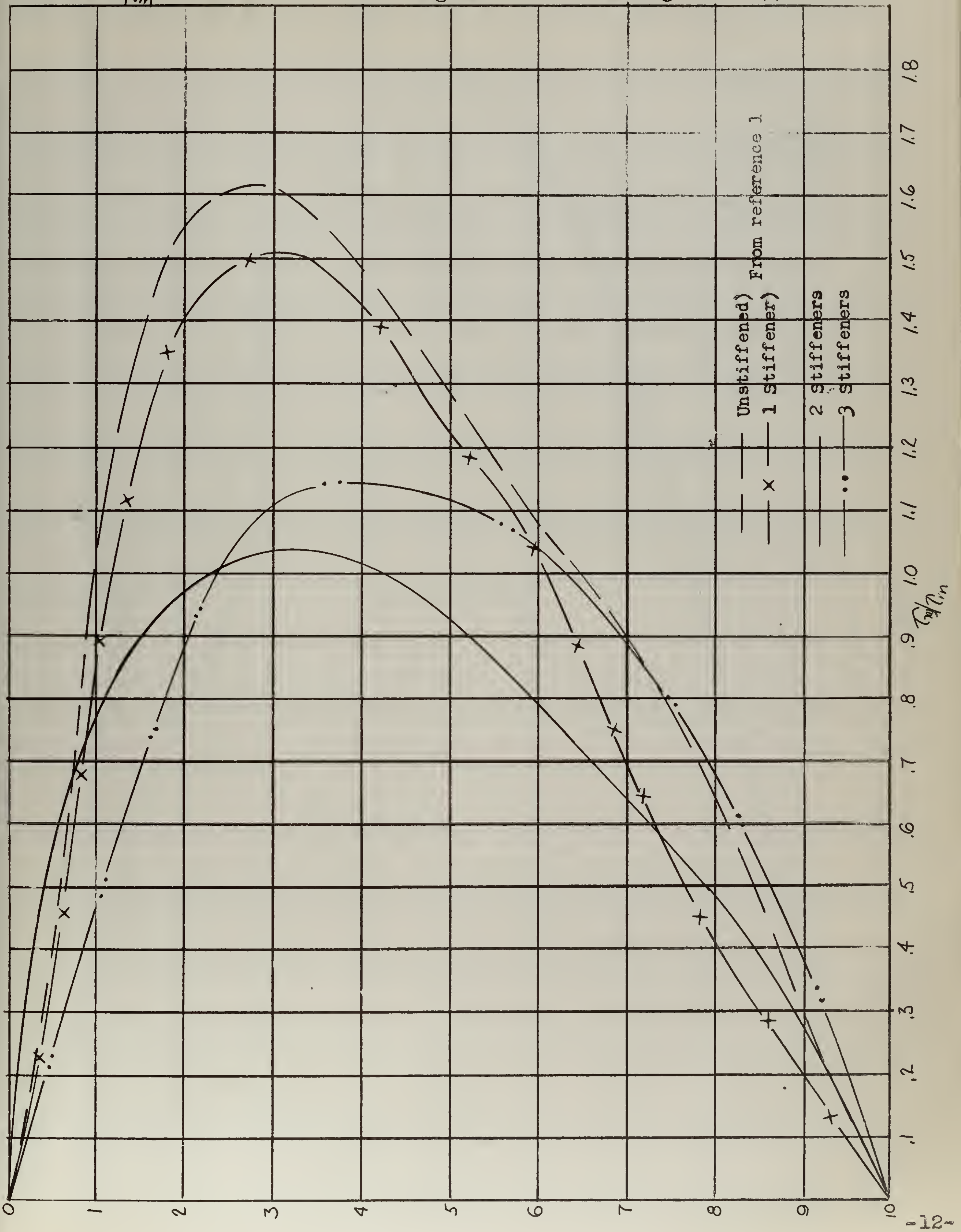

Figure V
Plot of τ_{xy}/τ_m for AR 3:1 for four degrees of stiffening and unsupported

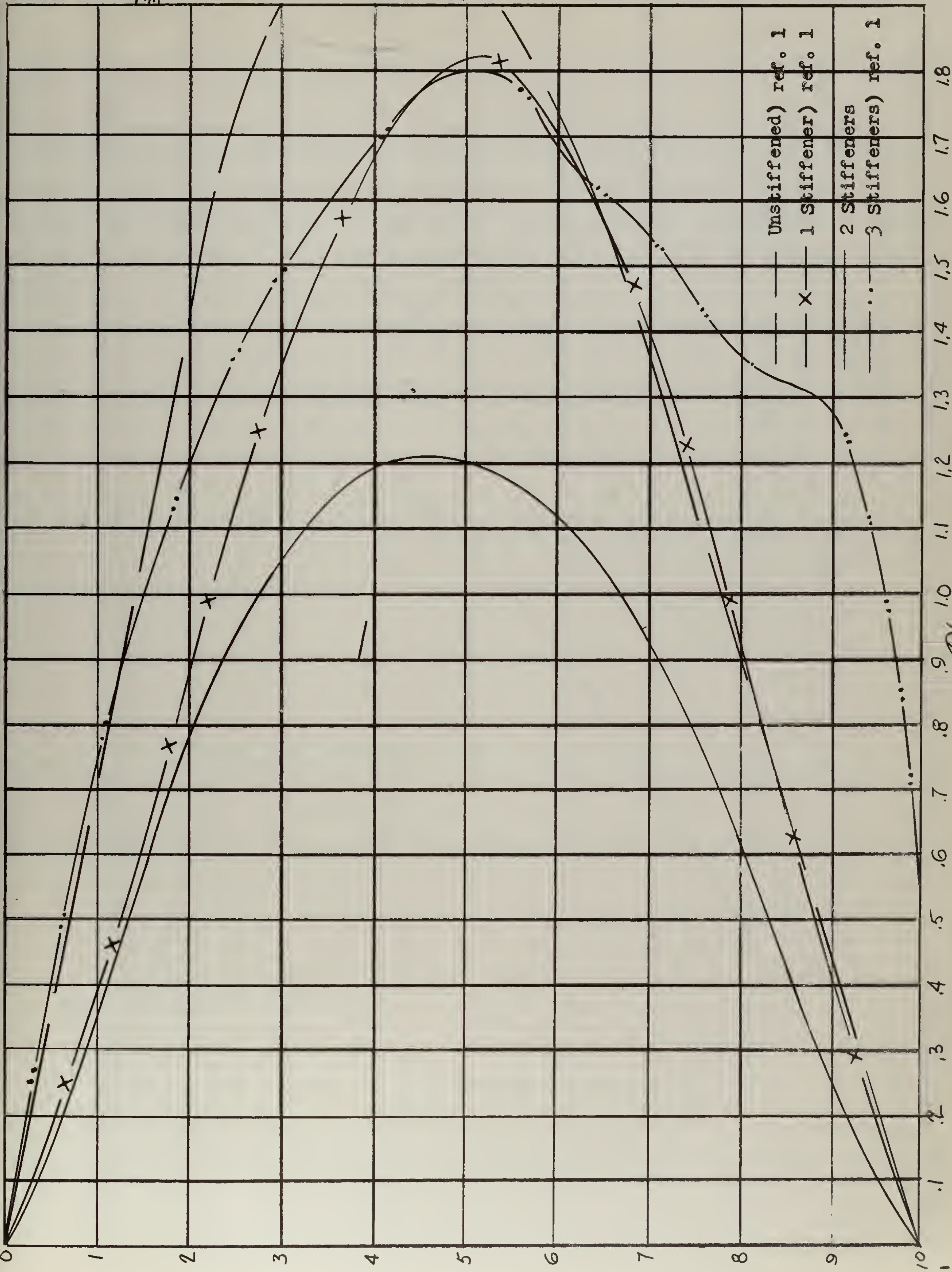

Figure VI

Plot of τ_{xy}/τ_m for AR 3:1 for four degrees of stiffening and supported

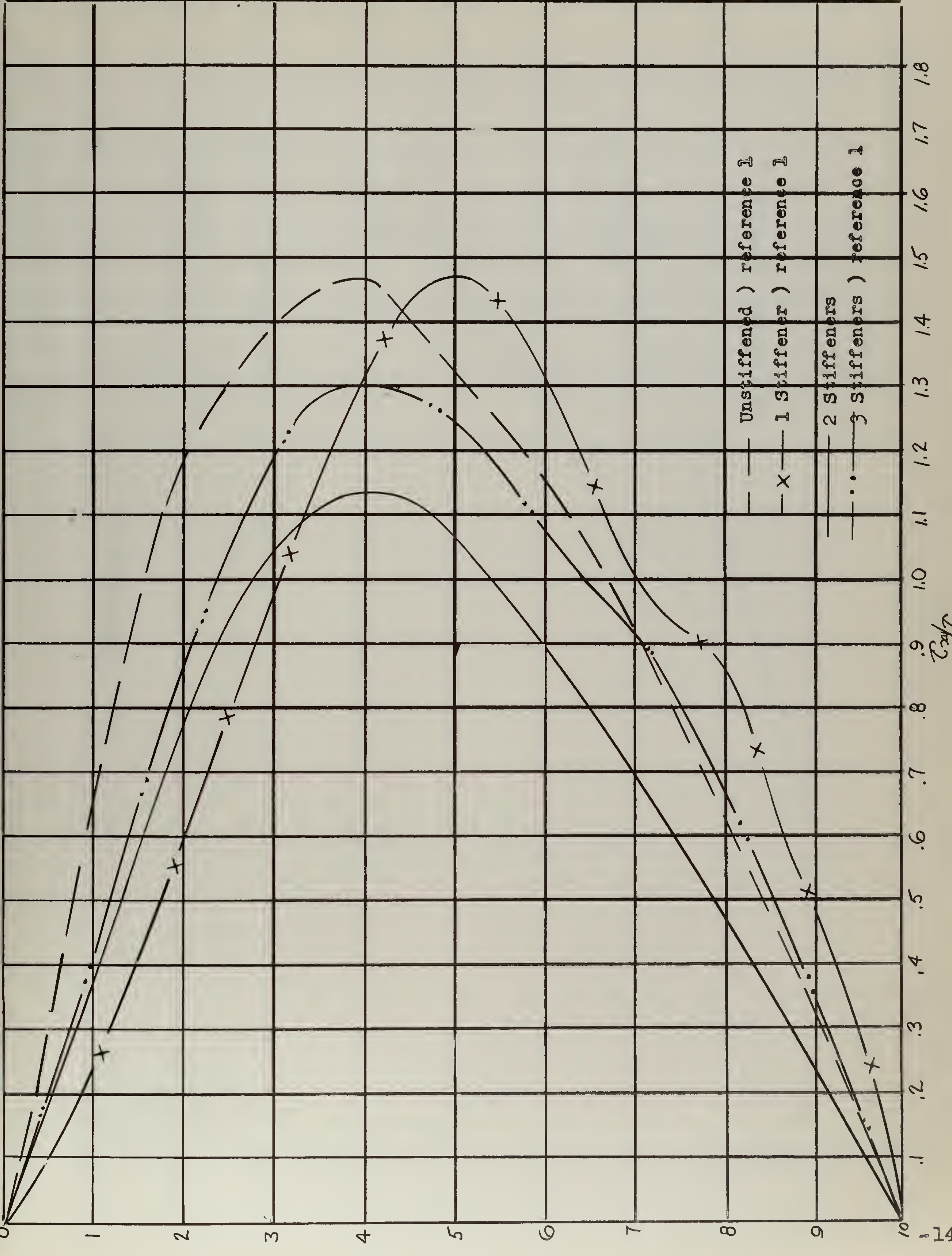

Figure VII

Plot of τ_{xy}/τ_m for AR 5:1 for four degrees of stiffening and unsupported

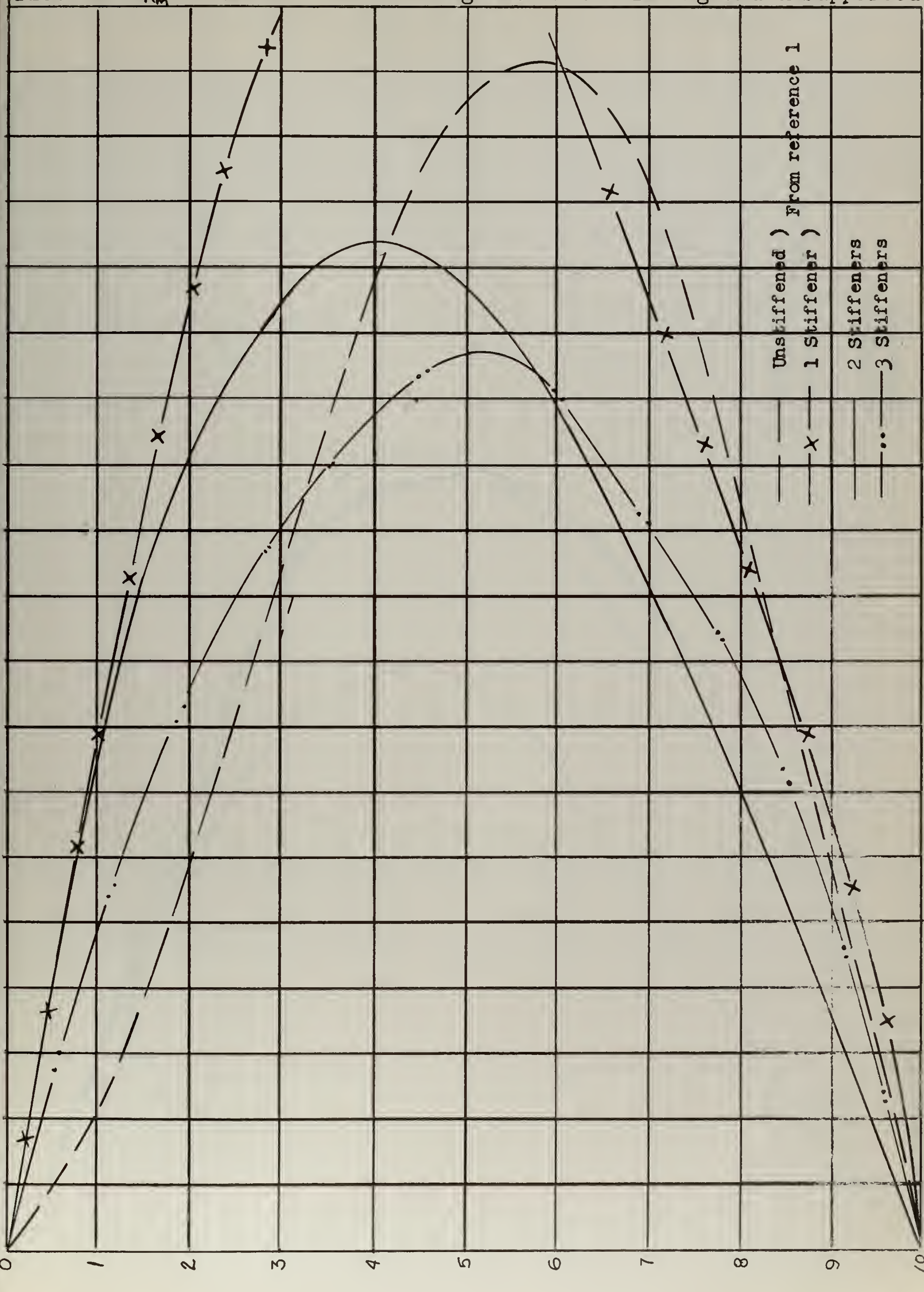

Figure VIII

Plot of τ_{xy}/τ_m for AR 5:1 for four degrees of stiffening and supported

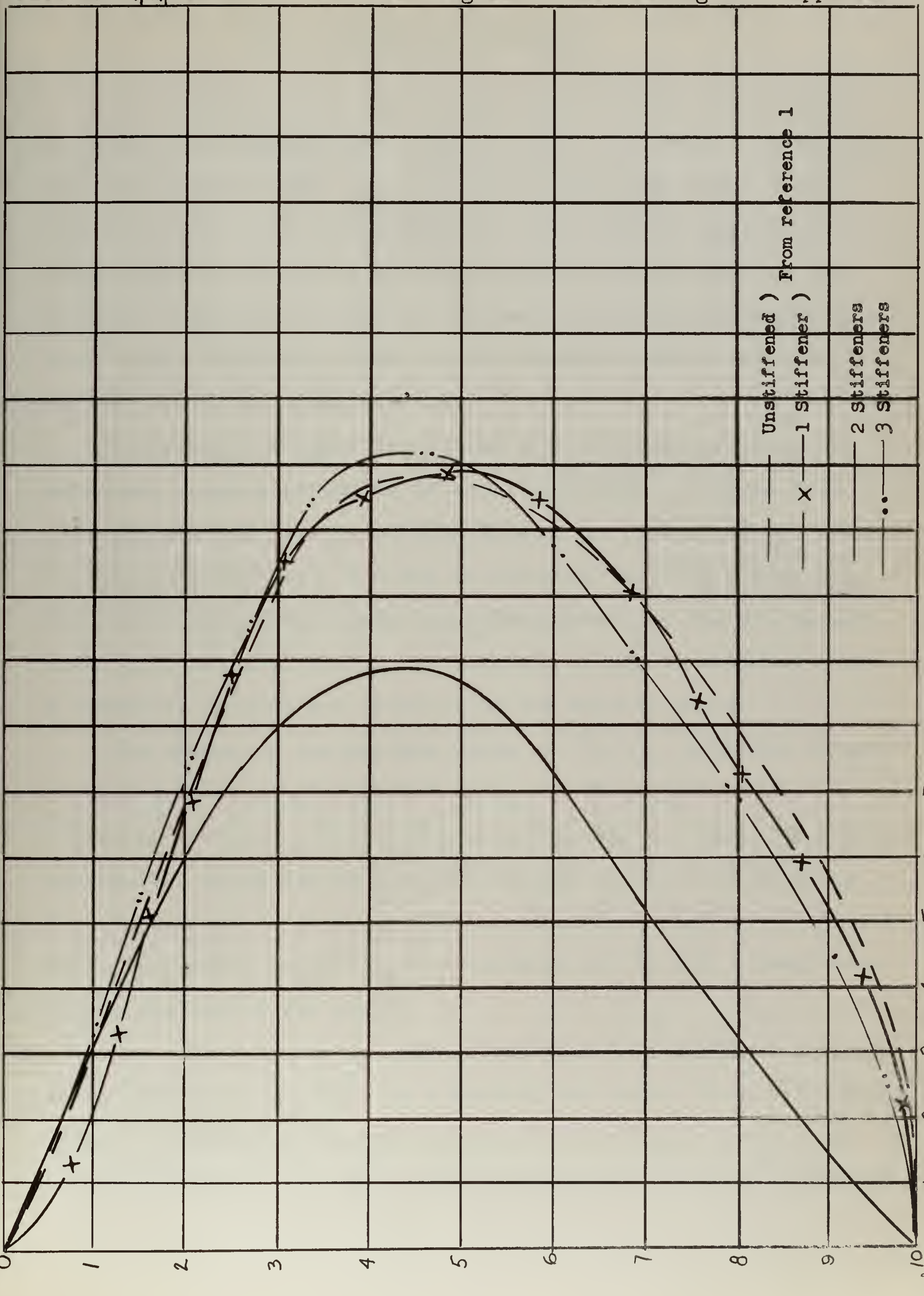

IV. DISCUSSION OF RESULTS

The results of the shear stress distribution were plotted by using the dimensionless ratio τ_{xy} / τ_m in order to facilitate the use of these data. It is felt that the mean shear stress that is present can be calculated if the expected distributed load across the top of a bulkhead and the contact area of one side of a bulkhead are known. Curves from these calculations should give numerical values of the expected shear stress at various locations along the end.

The general form of the stress distribution curves are as expected, roughly parabolic in shape. Figures I through VIII give the general results of this thesis, as well as of the work done in reference (1). It may be observed that the curves are very similar with the exception of the curve for the 3:1 aspect ratio with two stiffeners. In general, it may be observed that a symmetric loading was obtained in the several tests.

The change of the maximum value of τ_{xy}/τ_m with the change in aspect ratio is of especial note. As the aspect ratio decreased (from 5:1 to 1:1) the value of τ_{xy}/τ_m (max) decreased constantly, which can be explained by the behavior of shifting from deep beams to plates. Also it is noticed that as the aspect ratio decreased, the point of occurrence of τ_{xy} / τ_m (max) rose toward the top of the plate.

The effect of bottom support was that of reducing the total shear stress on the sides by a certain per cent. This percentage cannot be determined accurately because it varies widely from one aspect ratio to another. This amount of reduction definitely

shows a tendency to become smaller as the aspect ratio is decreased. At the 1:1 ratio, the difference between supported and unsupported is almost negligible. The bottom support in all cases also tends to raise the point of τ_{xy}/τ_m (max). This tendency may be considered to vary linearly as the aspect ratio decreases. The effect of increase in the number of stiffeners tends to decrease the value of (τ_{xy}/τ_m) and to distribute more shear into the bottom portion of the plate.

The accuracy of the tests was found by integrating the areas under the τ_{xy}/τ_m curves and comparing these areas with the area under the curve $\tau_{xy}/\tau_m = 1.0$. This, of course, could only be valid in the unsupported cases, since in the supported cases it was not known which part went into the bottom support and which part was attributable to inaccuracies. From the comparisons, the following percentage of error was found:

1:1	0 stiffener	3.9%
	1 stiffener	9.2%
	2 stiffeners	1.3%
	3 stiffeners	6.6%
2:1	2 stiffeners	1.5%
	3 stiffeners	14.0%
3:1	2 stiffeners	25.0%
5:1	2 stiffeners	2.6%
	3 stiffeners	11.2%

By disregarding the 3:1 case, it can be concluded that the over-all accuracy obtained for the tests is within 15%. The most inaccurate part of the experimentation is believed to have been in the determination of the isoclinic lines. These lines, in general, appeared as broad bands for some inclinations, and for other inclinations, seemed to mysteriously disappear at the most inconsistent places.

V CONCLUSIONS

The method of studying the stress distribution in deep beams by means of photoelasticity proved successful in this thesis.

It was found that the shear stress distribution along the clamped edges of the plate is nearly parabolic; this is more noticeable for large aspect ratios.

Bottom support will reduce the total shear stress on the sides; however this reduction is small for aspect ratios of 1:1 or lower.

The addition of one, two or three stiffeners to the models had very little influence in the direction of the principal stresses, for the same aspect ratio. The value of (τ_{xy} / τ_m) max decreases as the aspect ratio decreases. It was found that the bottom support tends to raise the point of occurrence of (τ_{xy} / τ_m) max.

Increase in the number of stiffeners tends to decrease the value of (τ_{xy} / τ_m) max. and to distribute more shear stress into the bottom part of the plate.

Except for one test (3:1 aspect ratio), the accuracy obtained was within 15%.

VI. RECOMMENDATIONS

The next field of endeavor should be the calculation of the percentage of bottom support that is present in the actual case of the ship bulkhead.

For further work in this field of loading plates, a combination of uniformly distributed loading and concentrated loading would be very interesting, though probably very difficult.

Better edge support will have to be found if plates of large aspect ratio are tested in the present loading frame.

A new and untried aspect ratio would not be recommended in view of the small difference obtained between those ratios already tested.

VII. APPENDICES

APPENDIX A

TECHNIQUES AND APPARATUS

1. Photoelasticity

Photoelasticity is an experimental method of determining, with the aid of polarized light, stresses in models made of certain transparent materials. Photoelastic stress patterns yield directly the tangential boundary stresses in two-dimensional problems and give a complete picture of the maximum shearing stress distribution within the interior.

Photoelasticity is based upon a phenomenon called "temporary double refraction", whereby certain transparent materials experience a change in optical characteristics when subjected to stress. This change is directly proportional to the intensity of stress and can be observed by using polarized light in a polariscope. A model is made geometrically similar to the prototype and is loaded in a similar manner. When examined in the field of polarized light of the instrument, alternate bright and dark bands are seen which can be interpreted in terms of stress.

In a plane-polarized field the directions of vibrations are all parallel to the one plane. For a circularly polarized field, the light vector rotates around the line of propagation, and its magnitude remains constant. It is also possible to speak of elliptically polarized light, of which circular polarization is a special case.

White light consists of a mixture of light of different frequencies, which can be distinguished from one another by the

eye. Monochromatic light consists of one wave length only, and it may be plane, circularly, or elliptically polarized. When a ray of light enters a doubly refracting material at normal incidence, it is resolved into two plane-polarized component rays which are transmitted on planes at right angles to each other. For these two waves, the indices of refraction are slightly different and the two rays travel through the material with different velocities and emerge with a slight shift relative to one another. A plane polarizer is a permanently doubly refracting material which transmits one of the component rays only. Hence the transmitted ray is plane polarized. The direction of these vibrations will be called the "transmission axis" of the polarizer.

Two plane polarizers with their transmission axes at right angles to one another form the heart of the plane crossed polariscope. With this arrangement, no light will be transmitted, since the second polarizer stops, plane-polarized beam produced by the first. When a photoelastic model is loaded, it becomes doubly refracting, and its transmission planes at any point coincide with the planes of principal stresses at that point. When a loaded model is placed in the field of the plane crossed polariscope, if the light is monochromatic, the two component plane-polarized rays vibrate in the directions of the principal stresses and have amplitudes dependent upon the principal stress directions. The two waves emerge from the model with a phase shift relative to one another, and this shift is proportional to the difference of the principal stresses at that point.

When the two rays reach the analyzer, their components parallel to the transmission axis of the analyzer pass through, while others are stopped. The relative phase shift produced during passage through the model is still present between these two waves and can give rise to interference effects. If the phase difference of the two horizontal components is zero or an integral number of wave lengths, the two waves cancel to give darkness. On the other hand, if the phase difference is one-half, three-halves, etc., wave length , the two waves add to produce maximum intensity. Thus the resulting image obtained from the polariscope is a series of light and dark bands. The dark bands are called "integral fringes" and have associated with them an integral number, called the "fringe order." The white bands would be the half-order fringes, since they correspond to relative retardations of odd multiples of one-half wave length . Each fringe is the locus of points of constant difference of principal stress.

Also, in the plane polariscope, at all points on the model at which one of the principal axes of stress is aligned with the transmission axis of the polarizer, the light ray passes through the model as one component, and no interference effects can be obtained. Regardless of the fringe order at such points, no light is transmitted by the analyzer. The black bands, called "isoclinics," are the loci of points of equal inclination of the principal stress. By rotating the polarizer and analyzer simultaneously, isoclinics of different angles may be obtained, and the direction of principal stress can be determined at any point.

In order to separate the isoclinics from the fringes, quarter-wave plates are added to a polariscope on either side of the model. A quarter-wave plate is a doubly refracting element which produces a phase difference of one-quarter wave length between the two emerging components. If a monochromatic light is used, and the quarter-wave plates have their axes set at 45° to the transmission axes of the polarizer, the emerging components recombine to produce circularly polarized light. The net result of using the quarter-wave plates is that the isoclinics are removed and the pattern on the screen consists of fringes only. Figure IX shows the optical arrangement of a standard circular polariscope.

In a polariscope in which the polarizer and the analyzer are so positioned that their planes of transmission are parallel, the resulting field will be of maximum brightness and a light field is present. When the two have their respective axes at right angles, a dark field will result.

In analyzing a fringe pattern, one must be able to assign correct fringe orders to the interference bands. If a monochromatic light is used, the integral fringes will be the same as the background; dark for dark field, and light for light field. The fringe order at a selected point can be determined by observing the pattern as the load is applied.

It often happens that the maximum fringe order is not an integer but some fractional part between two integral fringes. In such a case it may be necessary to have the exact fringe order. The Tardy method of obtaining fractional order was used in this

Figure IX

Standard or Crossed Polariscope

Monochromatic Light Source

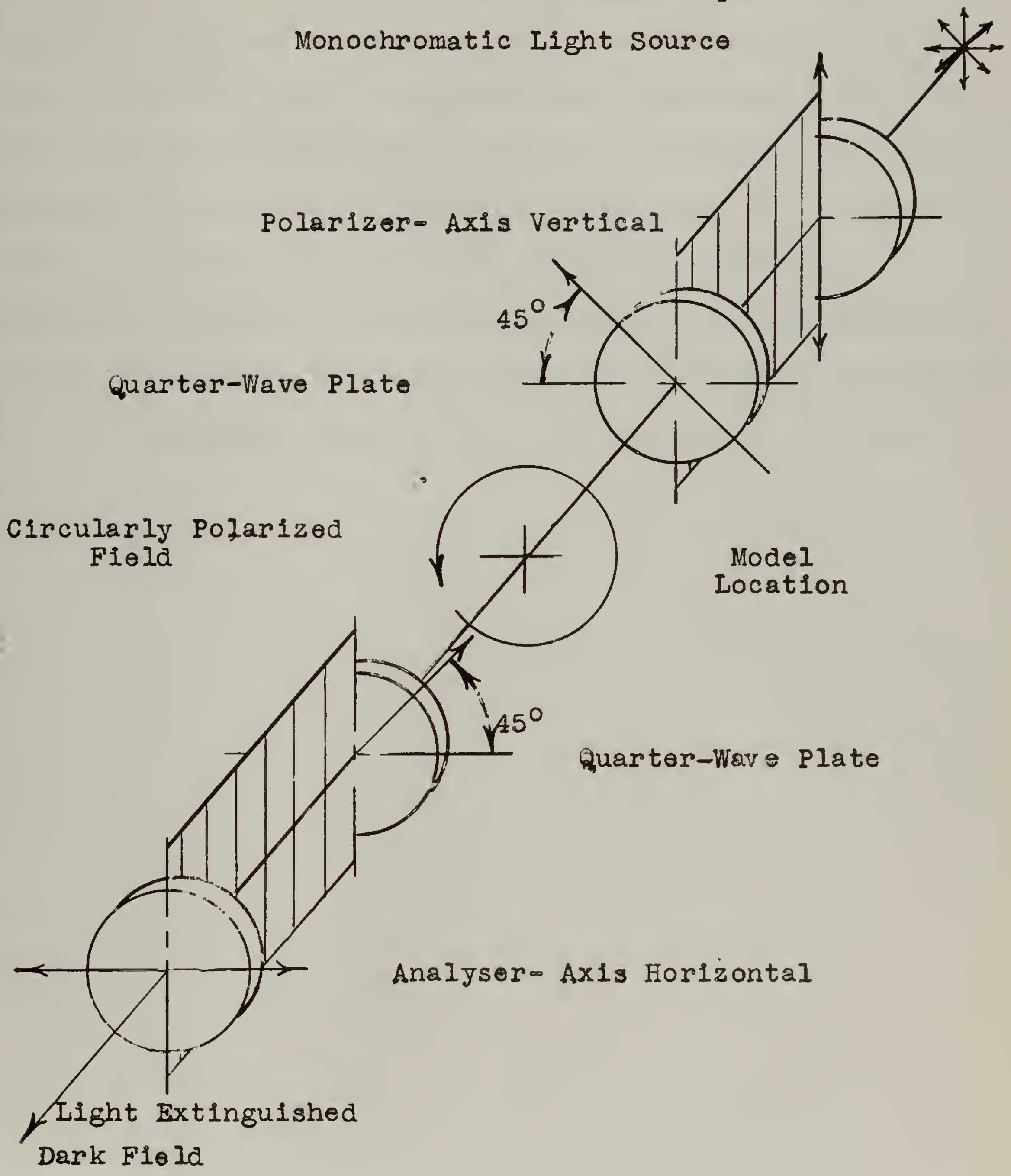

thesis. By rotation of either the polarizer or the analyzer the integral orders may be made to move toward the half-orders. Since a rotation of 90° of either will change the field from either a dark one with dark fringes to a light one with light fringes, 90° rotation is equivalent to moving the fringe one-half order. Any fraction of 90° rotation results in a comparable fraction of the one-half order. If the analyzer is rotated 45° to make the fringe advance to the point of interest, then the fractional order will be one quarter of an order.

2. <u>The Polariscope</u>

This thesis was conducted in the Ship's Structure Laboratory of the Department of Naval Architecture and Marine Engineering. The polariscope installed in the laboratory is model No. 402, manufactured by the Polarizing Instrument Company. The polariscope is pictured in Figure X.

The polariscope is physically divided into two parts, one on either side of the model location. Each part consists of a two-tracked optical bench supported by legs on which is attached the polarizing equipment. The part containing the light source is called the light-source bench and includes the light source, the collimating lens, the polarizer, and the quarter-wave plate. The analyzer bench, on the other side of the model, consists of the analyzer and its associated quarter-wave plate, another collimating lens, a filter, the camera lens, and the camera itself.

The light source has an arrangement to supply either white light of 300 watts or mercury vapor light of 5461° A. Also there is an arrangement for the use of two apertures, one 1.5 mm. in diameter, and the other 3 mm. in diameter. Normally, for the study of isochromatics, the small hole is used with the mercury light. The large hole is used with white light for the study of isoclinics.

The collimating lens on the light-source bench is used to convert the divergent light rays into parallel rays. It is placed between the light source and the polarizer.

Figure X - The Polariscope

Last on the light source bench is the polarizer and its associated quarter-wave plate. Both polarizer and quarter-wave plate may be rotated through 180° independently. When the angle indicators of each are on the same value, the quarter-wave plate is oriented 45° from the plane of transmission of the polarizer. When the polarizer is set at 90°, the plane of polarization is vertical. The quarter-wave plate is mounted on a pivot and is easily rotated out of the path of light to produce a plane polariscope.

After passing through the model, the light strikes first the quarter-wave plate and associated analyzer. This group is similar to the polarizer and quarter-wave plate in that both may be rotated through 180°. Also, when both the analyzer and the quarter-wave plate indicate the same angle, the plane of transmission of the analyzer is 45° from the plane of the quarter-wave plate. When the analyzer is positioned at 90°, the plane of transmission is horizontal. When all units, both quarter-wave plates, polarizer and analyzer are set at 90°, a circular polariscope with dark field as indicated in Figure IX will result.

The collimating lens is inserted after the analyzer to focus the parallel light rays to a point at the camera lens. After the collimating lens there is installed a filter (Wratten #77) and then the camera lens and the camera. The shutter on the camera can be adjusted and the speed of the shutter may be regulated from 1/50 of a second to ½ of a second. In the rear of the camera is a removable ground-glass screen. In place, it is used to present a clear visible picture of the isochromatics and isoclinics. A film holder is available to insert between the lens and the screen. This holder takes cut film of 8" x 10" size.

Also provided is a tracing attachment with installed mirror set at 45° for tracing patterns onto paper. Before this tracing attachment is installed, the film holder and the ground-glass screen must be removed.

3. The Loading Device

The uniform loading device used in this thesis was made last year by the students that initiated the present work. (Ref. 1). This device is pictured in figure XI and the plans and dimensions are indicated in figure XII. It consists of a gum rubber tubing 3/8" in diameter inserted in a rectangular slot of a steel plate. The tubing is connected through a coupling to a hydraulic pump which puts oil pressure inside the tubing.

The top edge of the models was located in the slot securely against the rubber tubing and then the pressure was applied. The pressure in the tubing was measured by two gauges, one connected to the loading device, and the other connected on the end of the pump. The gauge connected to the loading device was considered to be more accurate, as there is a check valve in the oil line between the loading device and the pump which would not permit a drop in pressure to be readily observable at the pump.

Another modification to the loading device as used last year was made to be able to perform tests on models of shorter length. This consisted on the welded addition of piece 1 (see Figure XII) after the long models had been tested. The drilling of eight additional holes in the steel plate was also necessary

Figure XI - Uniform Loading Device

Figure XII

Uniform Loading Device

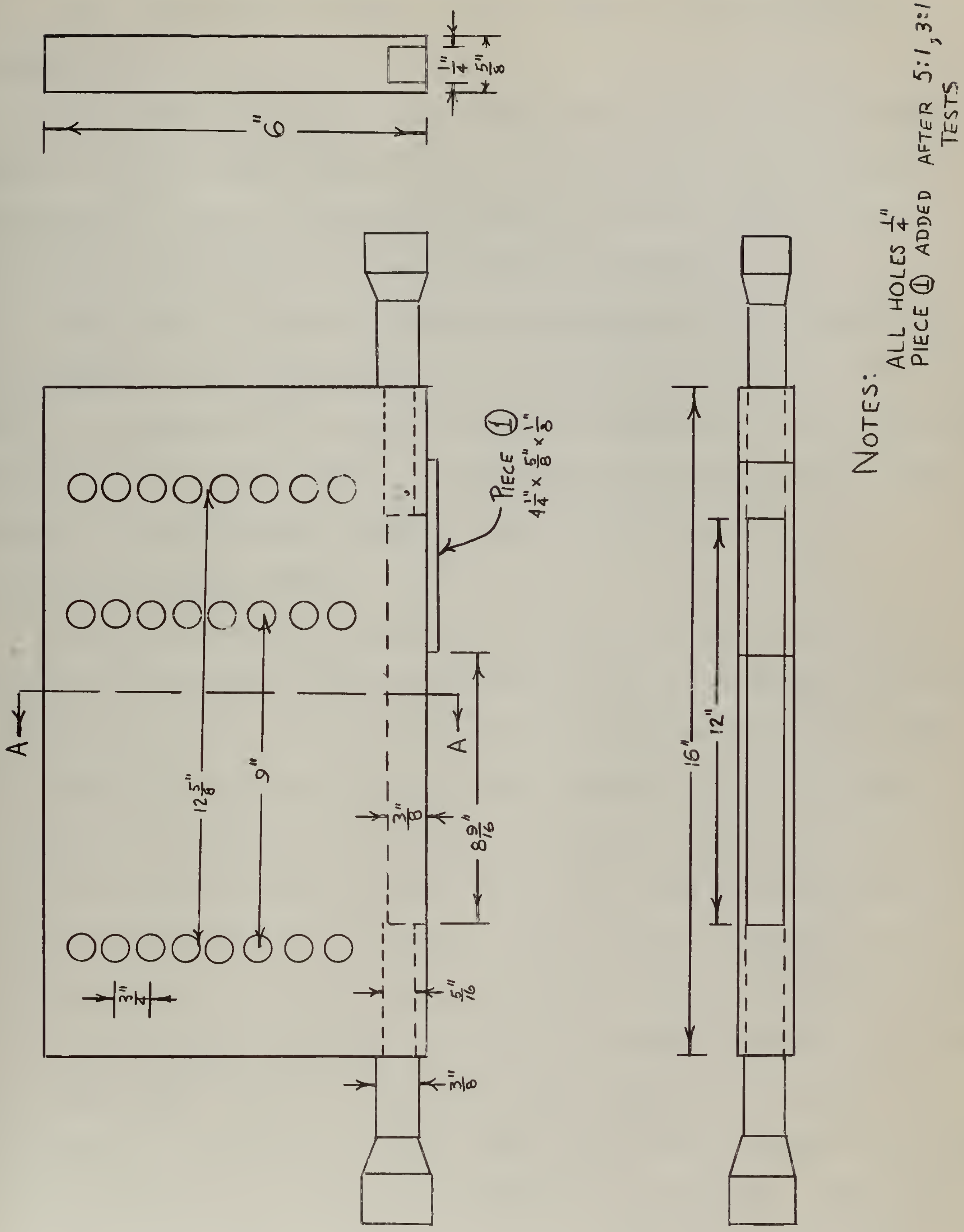

to fit the loading device into the straining frame.

The calibration of the loading device is explained in Appendix D.

The deterioration of the rubber tubing due to the presence of the oil and high pressure was a problem and there was much experience gained in the installation of this tubing. The procedure described in reference (1) was followed.

This type of loading device, in general, may be considered satisfactory for this type of experimentation; however, it would not be recommended for models whose thickness would be less than .230" nor more than .260". A more detailed description of the constructional features may be found in reference (1).

4. The Straining Frame

The straining frame used for the tests in this thesis was especially designed and constructed for the experimental work of reference 2, and it has been in use for references (1), (2), and (3). The frame, see Figure XIII, consists mainly of four vertical supports constructed of structural aluminum channels. Since all the work was done with uniform loads, the same method employed in reference (1) was used. The models were clamped between the two channels at either end by means of steel bolts spaced 7/8" apart. In order to obtain as much friction as possible between the model and the frame, 3/16" steel chocks were inserted on either side of the model. In addition, emery paper was placed between the model and the chocks to improve the clamping of the model. The bolts to secure the model were then drawn up uniformly as tight as possible.

When the test of models of aspect ratios 5:1 and 3:1 were finished, the loading frame was modified by relocating two of the channels at a distance of 6" from the other two. This step, in addition to the modification to the loading device, (see appendix A) permitted the use of six-inch models. With this change the tests for aspect ratios of 2:1 and 1:1 were made.

For experiments of this thesis it is felt that a better clamping of the ends was obtained than that obtained in reference (1). However, the certainty of perfect clamping cannot be assured. A complete description of the frame, including its construction plans can be found in reference (2).

Figure XIII - Loading Frame

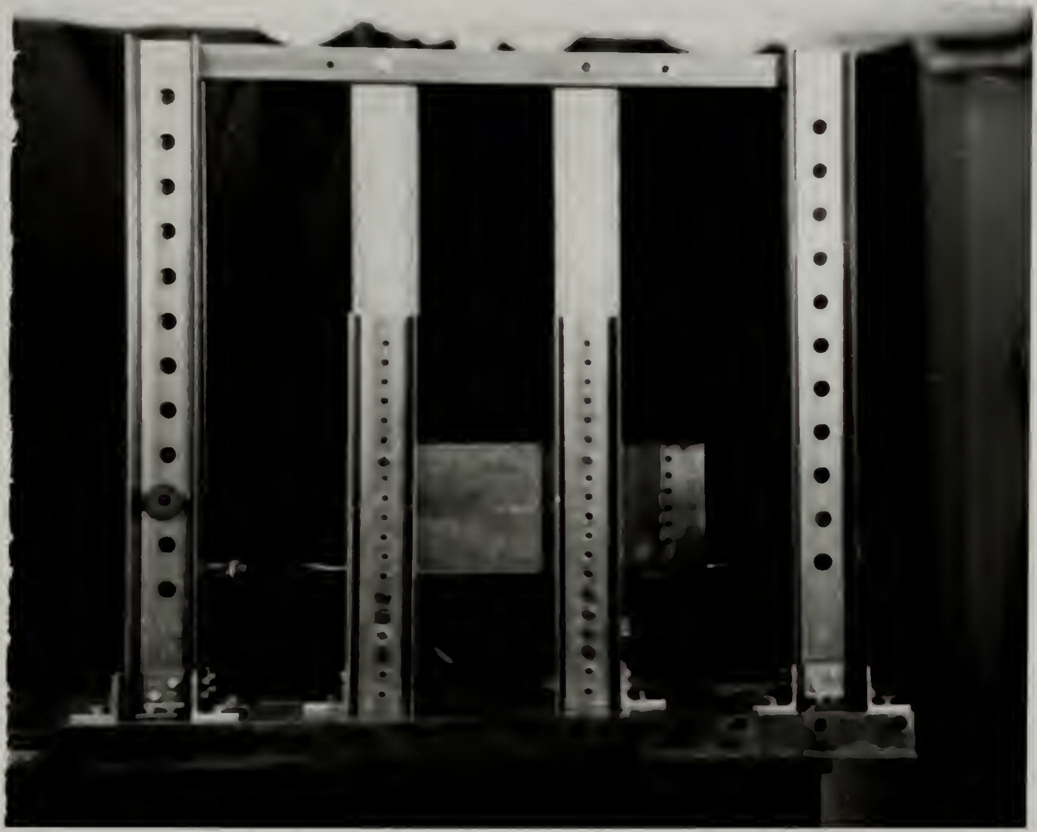

Figure XIV - Model Samples

APPENDIX B

DETAILS OF PROCEDURE

1. Preparation of the Models

The photoelastic materials for this thesis were selected with two ideas in mind. First, it was desired to have a material with a low fringe constant in order to obtain a large number of isochromatic lines in all the tests. Secondly, since this thesis is a continuation of the work started in reference (1), material very similar to that which was used in that reference was used to obtain uniformity in results.

The material used for obtaining the isochromatics was Catalin 61-893, which is a special cast resin that is easily machined with standard tools and possesses a good combination of mechanical and optical properties. This material was delivered already polished and annealed, thus facilitating the work to be done by the authors.

The material used for determining the isoclinics was plexiglas as it has a low sensitivity. The material was delivered ready to use.

Models for the eighteen (18) isochromatic tests were made for aspect ratios 1:1, 2:1, 3:1 and 5:1. For the latter two aspect ratios the models were made with over-all length equal to twelve inches. For the other aspect ratios the over-all length was eight and one-half inches. Due to damage to one of the plates of Catalin purchases for this thesis, the material used for the tests for isochromatics for aspect ratios 5:1 and 3:1 was Catalin which was left from the stock

purchased for reference (1). For the tests of these models the fringe constant obtained in reference (1) was used.

The stiffeners were made of the same material as the model, and in all cases were $\frac{1}{2}$" x $\frac{1}{4}$", and were of the same height as the model less $\frac{1}{4}$" for allowing the model to enter the loading device. For the purpose of cementing the stiffeners to the models, Penacolite adhesive G1124 was used with good results. The stiffeners were allowed a setting time of at least 24 hours, as this was recommended by the manufacturer of the Penacolite. Two sets of stiffeners were used, one set on each side of the model. This permitted more uniformity and insured that no bending resulted.

Rounded edges were specifically avoided along the top edge of the model. Cutting of all models was done first on a high speed saw of within .05" of the final dimension and then on a high speed vertical mill to the final size. Light emery paper was needed to finish the cut edges. A final polish with Nujol was given to remove any scratches, dirt or fingerprints.

2. Sequence of Testing

The first step in the procedure of testing was the insertion of the aluminum bar stock in the loading frame. This bar was placed on bolts inserted through the loading frame for ease in removing after the test. Next, the Catalin model was inserted on top of the bar and the loading device was placed on top of the model. Bolts were inserted to hold the loading device up while the steel chocks and emery paper were installed on each side of the model in the clamping region.

Bolts were then inserted to hold the model in position but care was taken not to tighten these too much. The bolts holding the loading device and the aluminum bar were then tightened as much as possible. The white light was turned on and the model was positioned so that the presentation on the ground-glass screen showed clearly one edge (for models 6" long the whole model was shown on the screen). The mercury light was then turned on and into position. While it was warming up, the quarter-wave plates were pivoted into position and set to 90°. The polarizer and the analyzer were also set to 90°. The hydraulic pump was connected to the loading device and lines checked for leaks.

A load of 40 psi was then put on the loading device to adjust the model in the frame. At this point the model was rigidly tightened in the frame.

While the pressure in the loading device was being brought up to the testing pressure, the isochromatic pattern was being observed on the ground-glass screen to determine the order of the various fringes. When at testing pressure the film holder was inserted into the camera and a picture of the isochromatics was taken. While this was being developed in the dark room the Tardy method was used to determine the fractional orders at the scribed points along the end of the model.

When it was ascertained that the picture was satisfactory, the mercury light was extinguished and the pressure was withdrawn.

To prepare the model for test without bottom support the only work necessary was to remove the bolts supporting the

aluminum bar. The bar could then be lowered out of the way and the test conducted. This test was then the same as previously described.

On completion of the bottom unsupported case, the Catalin model was removed from the frame and the Plexiglas model similar to the first was inserted in the same manner as was the Catalin. The mercury light was rotated out of the way and the white light was turned on. Quarter-wave plates were pivoted out of the light path, the filter was removed from the camera lens and the tracing attachment replaced the ground-glass screen. The large aperture was rotated into position and then the polarizer and analyzer were set to be 90° apart so that all the light striking the analyzer was transmitted. The outline of the model could then easily be traced onto the tracing paper. The pressure was then brought up to the same testing pressure as was used in the Catalin test. Next, the polarizer and analyzer were set both on 90°. Then systematically both were rotated together at 10° intervals through 90° while the isoclinics were sketched for each 10° step.

The unsupported test was then just as easy to set up as in the isochromatic case, just by removing the bolts supporting the aluminum bar stock.

On completing the tests for aspect ratios f:1 and 3:1 the loading frame was moved so that there was six inches between the upraised supports. The remaining aspect ratios were then tested in this position by the repetition of the above steps.

3. Photography

To obtain the pictures presented in Appendix E, the polariscope provides a camera that uses a standard 8" x 10"

cut film. The lens arrangement is composed of a lens proper and a green filter (Wratten #77). The lens can be moved along the length of the tracks and also small adjustments can be made by means of a pinion arrangement on the lens.

White light is passed through the system and the camera lens is placed where the second collimating lens focuses the light to a point right in the center. If the point of light does not hit the camera correctly, the tracks must be aligned either horizontally or vertically.

After placing and securing properly the forward part of the camera, the ground-glass screen was placed at the correct location by obtaining the desired size of the image. The position of the screen has nothing to do with the focus of the model image. Exposure speeds of 1/5 and 1/2 of a second were used with better results obtained with the latter speed.

The film used was Kodak Royal Ortho cut film 8" x 10" in size. This film has good sensitivity to green light. The small aperture (1.5 mm.) on the masking plate of the light source was always used. The negatives were developed immediately using developer Kodak DK 60A. Finally, the negatives were printed on 8½" x 11" Kodak Kodabromide AZO F3 and F4. This was done on the contact printer located in the Ship's Structure Laboratory.

APPENDIX C

DETERMINATION OF THE FRINGE CONSTANT

The fringe constant of the material was determined by the use of tensile specimen manufactured from a plate of the Catalin. The fringe constant "f" of a material at a given temperature and for a given wave length of monochromatic light is given by the relation

$$f = \frac{(\sigma_1 - \sigma_2)\ h}{n}$$

where σ_1, σ_2 = principal stresses

h = thickness of material

n = order of interference at the point where σ_1 and σ_2 are measured

If a tensile specimen is in use, one of the principal stresses becomes equal to zero, and the other may be determined by the geometry of the specimen and the load applied. The thickness of the model can be measured and the order of interference "n" can be found by observing the changes from dark to light in the model,while the load is being applied. These changes will occur in the model while in a circularly polarized field using monochromatic light.

In this thesis the loading frame from the Experimental Stress Analysis Laboratory was used for this determination. The load applied was measured with a Baldwin load cell, and the load was recorded for each order. Two runs were made and the average was used for plotting the slope of the curve.

From the curve, the fringe constant was calculated to be 92.8 lb/in-order.

Table I

Determination of Fringe Constant

Order	Indicator reading	ΔGR	Indicator reading	ΔGR	Average ΔGR	Load lbs
0	0-10-0985	*	0-10-0970	*	*	0
1	10-1100	0115	10-1090	0120	0117	11.7
2	10-1490	0505	10-1490	0520	0512	51.2
3	10-1910	0925	10-1890	0920	0922	92.2
4	12-0330	1345	12-0305	1335	1340	134.0
5	12-0740	1755	12-0720	1750	1752	175.2
6	12-1130	2145	12-1130	2160	2152	215.2
7	12-1550	2565	12-1530	2560	2562	256.2
8	12-1940	2955	12-1935	2965	2960	296.0
9	14-0335	3350	14-0350	3380	3365	336.5
10	14-0735	3750	14-0740	3770	3760	376.0

Baldwin SR-4 Strain Indicator Type L Serial #H80797
Baldwin SR-4 Load Cell Type U Serial 500

Tensile Specimen :

h= 0.268"

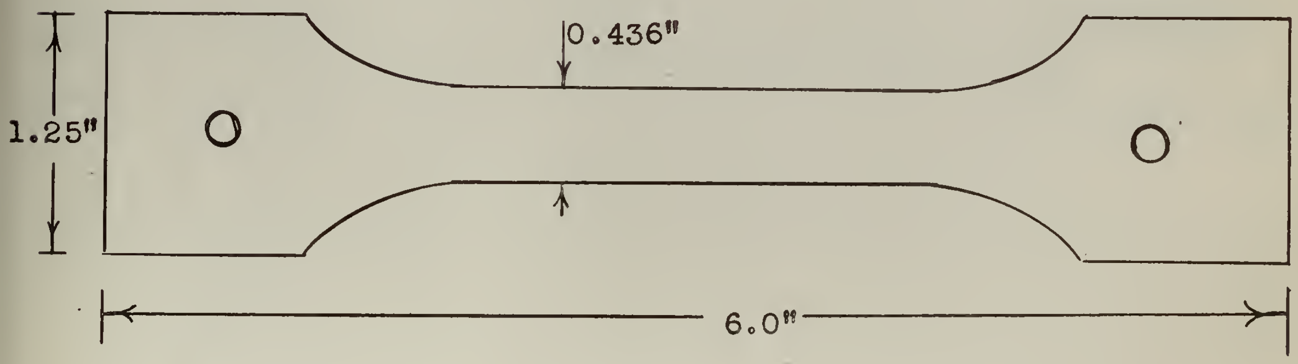

Figure XV

Calibration of the Material

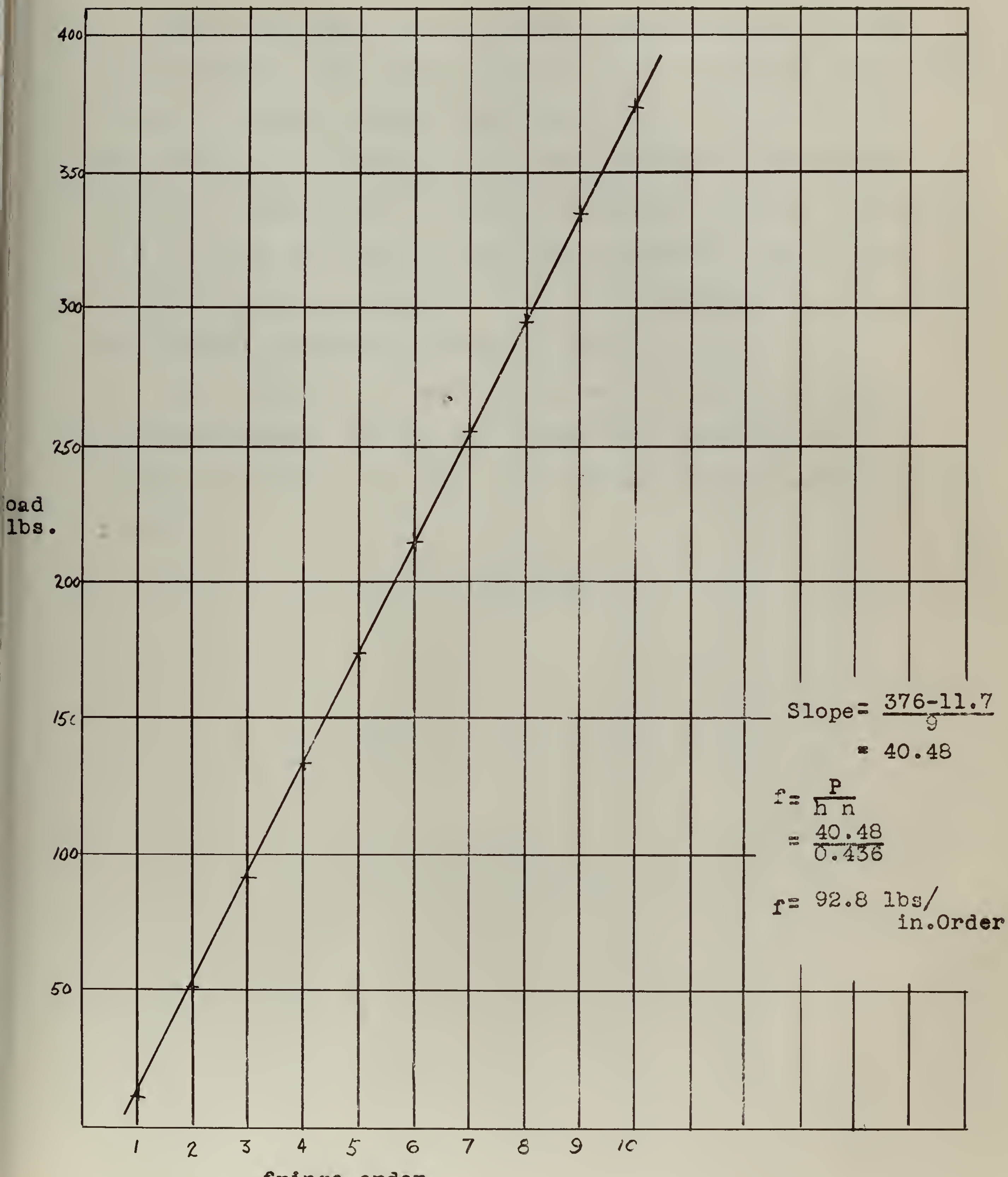

APPENDIX D

CALIBRATION OF THE UNIFORM LOADING DEVICE

The calibration of the uniform loading device was made by two methods, one consisting of a simply supported beam, twelve inches in length, supported one-half inch from the ends. By this method only points in the lower region of the applied load were obtainable. The limit of applied load was considered to be roughly 250 psi. for fear that excessive loading would rupture the test specimen or that the deflections would be such as to cause the rubber tubing to break.

The second method used consisted of a cantilever beam as indicated below. The end not clamped was supported by a Baldwin Load Cell from which the load was easily computed by the formula

$$w = \frac{8 \times R_1}{3 \times l}$$

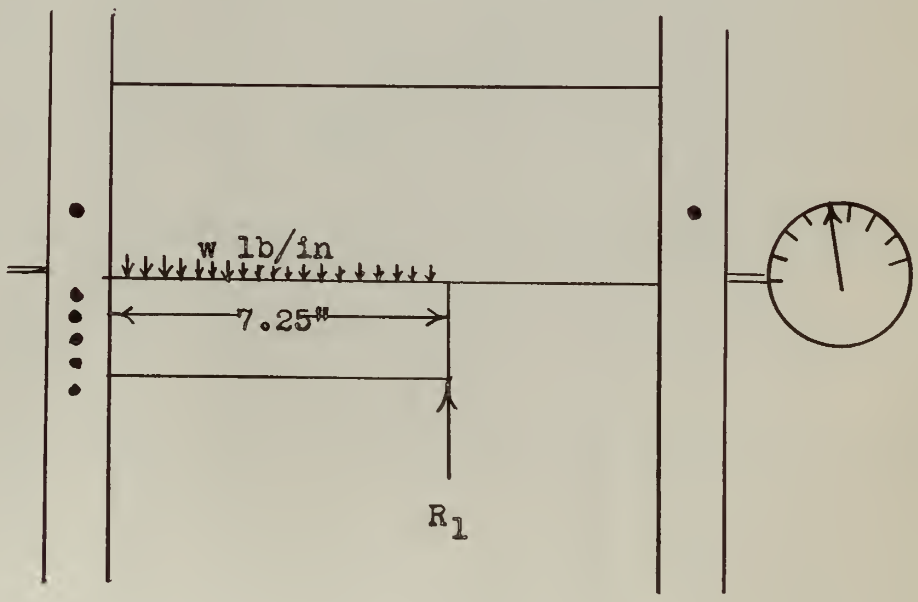

Table II

Calibration of Loading Device

Applied pressure	Indicator reading	ΔGR	R_1 lbs.	w lbs/in	psi
0	0-10-0555		0	0	0
50	10-0490	0065	6.5	2.39	50
100	10-0187	0368	36.8	13.53	100
150	8-1824	0721	72.1	26.52	150
200	8-1426	1119	111.9	41.15	200
250	8-1010	1545	154.5	56.82	250
300	8-0611	1944	194.4	71.50	300
350	8-0140	2415	241.5	88.70	350
400	6-1700	2855	285.5	105.00	400

Baldwin SR-4 Strain Indicator Type L Serial #H80797
Baldwin SR-4 Load Cell Type U Serial 500

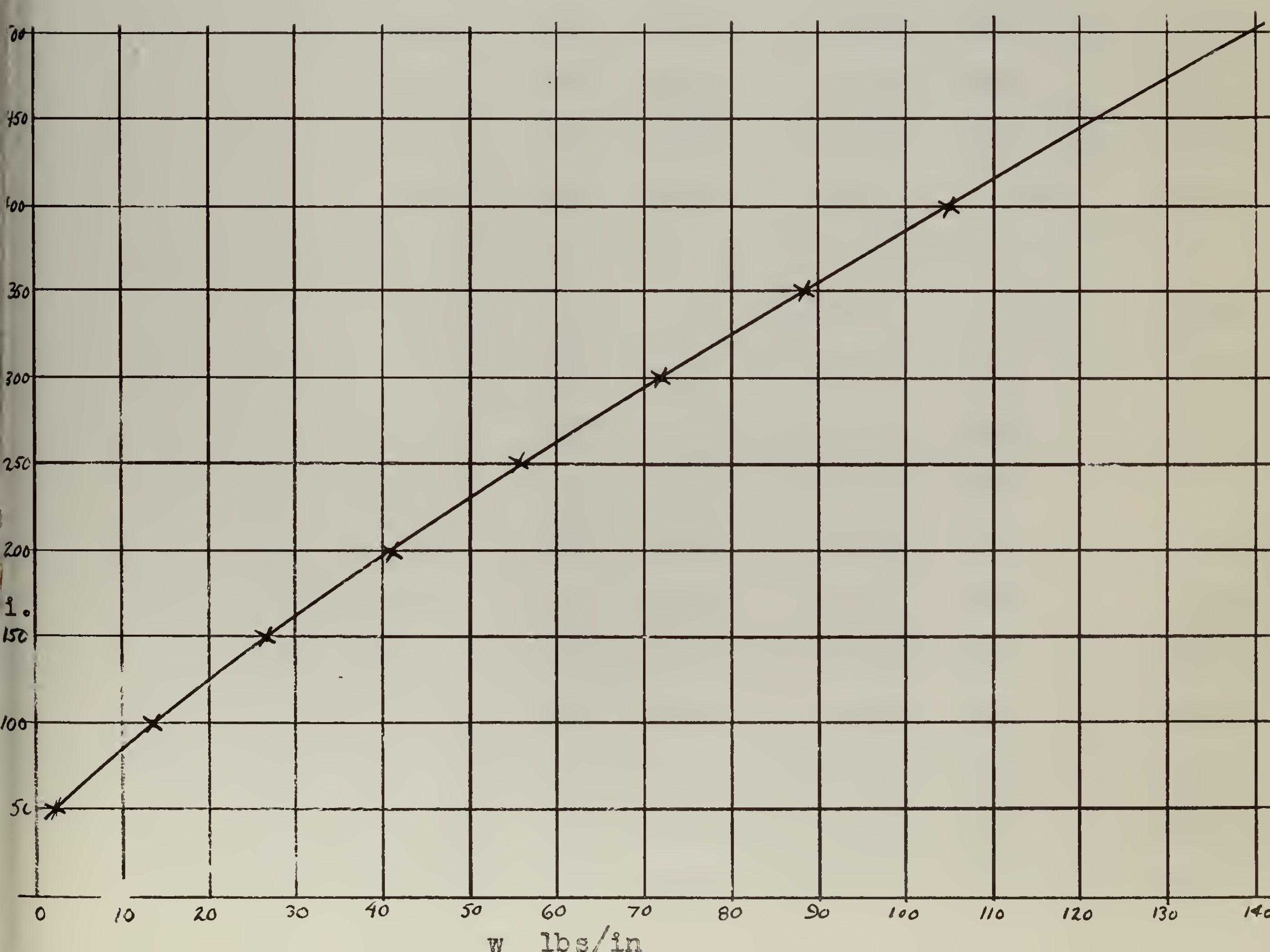

APPENDIX E

Original Data and Calculations

TABLE III

Aspect ratio 1:1 0 Stiffeners

Load 500 psi.

Bottom Unsupported

Station	Order	θ	2θ	Sin 2θ	τ_{xy}	τ_{xy}/τ_m
0	0.5	0°	0°	0.00	0.00	0.00
1	1.8	34°	68°	.8987	299.	1.07
2	2.4	43°	86°	.9975	443.	1.58
3	2.5	47°	94°	.9975	461.	1.64
4	2.5	49°	98°	.9902	458.	1.63
5	2.3	52°	104°	.9703	413.	1.48
6	2.0	55°	110°	.9396	348.	1.245
7	1.6	58°	116°	.8987	266.	0.95
8	1.1	62°	124°	.8290	168.	0.60
9	0.3	70°	140°	.6427	35.	0.13
10	0.0	90°	180°	.00	0.00	0.00

Bottom Supported

Station	Order	θ	2θ	Sin 2θ	τ_{xy}	τ_{xy}/τ_m
0	0.5	0°	0°	0.00	0.00	0.00
1	1.8	40°	80°	.9448	315.	1.14
2	2.3	47°	94°	.9975	424.	1.51
3	2.5	52°	104°	.9703	449.	1.60
4	2.3	54°	108°	.9510	405.	1.45
5	2.0	56°	112°	.9271	343.	1.23
6	1.6	58°	116°	.8987	266.	0.95
7	1.1	61°	122°	.8480	172.	0.61
8	0.6	65°	130°	.7660	85.	0.30
9	0.2	70°	140°	.6427	23.	0.08
10	0.0	90°	180°	0.0	0.0	0.0

Figure XVII

Sketch of the Isoclinics and Data for
AR 1:1 unstiffened and unsupported

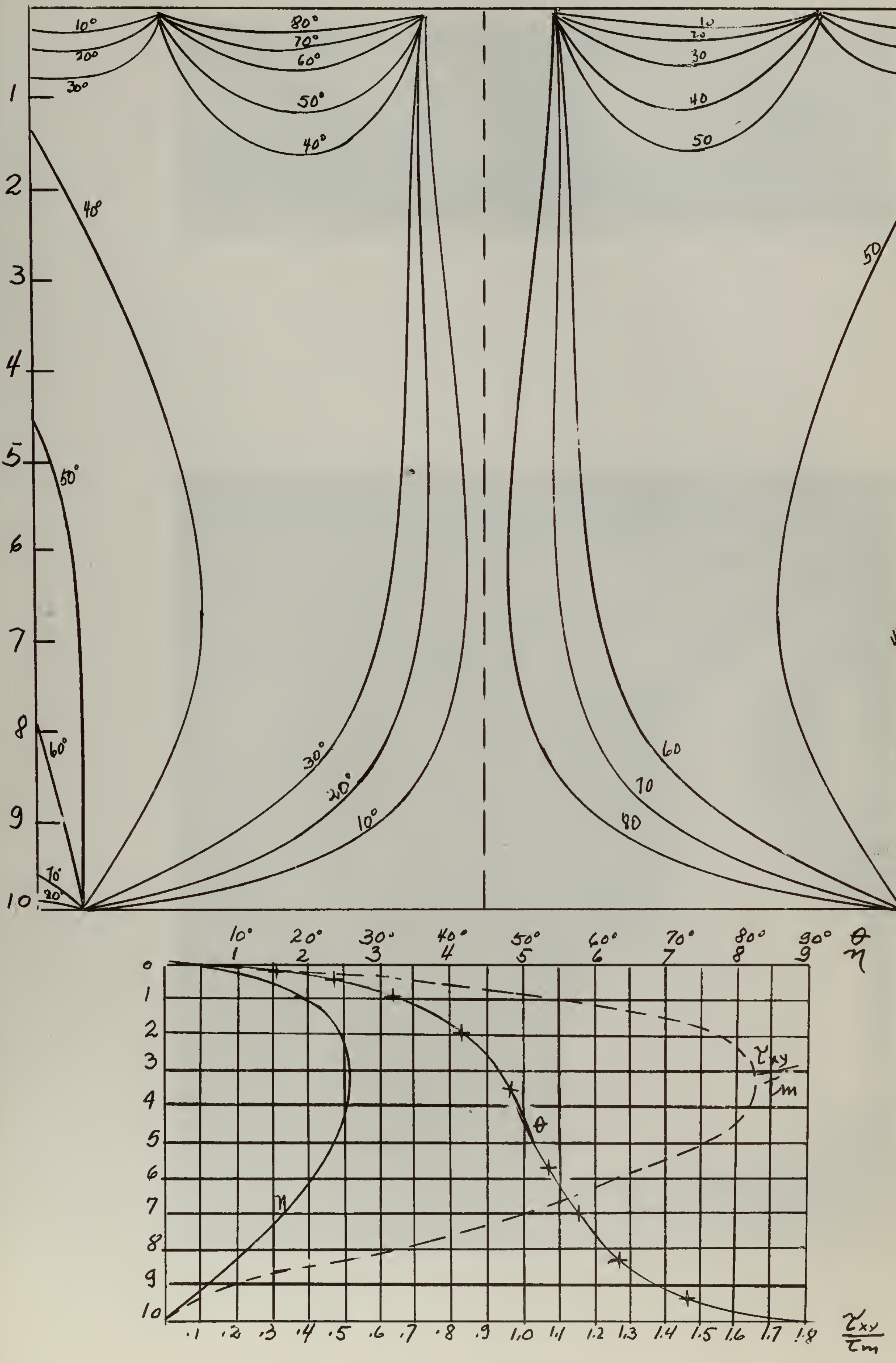

Figure XVIII

ASPECT RATIO 1:1

UNSTIFFENED

Figure XIX

Sketch of Isoclinics and Data for AR 1:1
unstiffened and supported

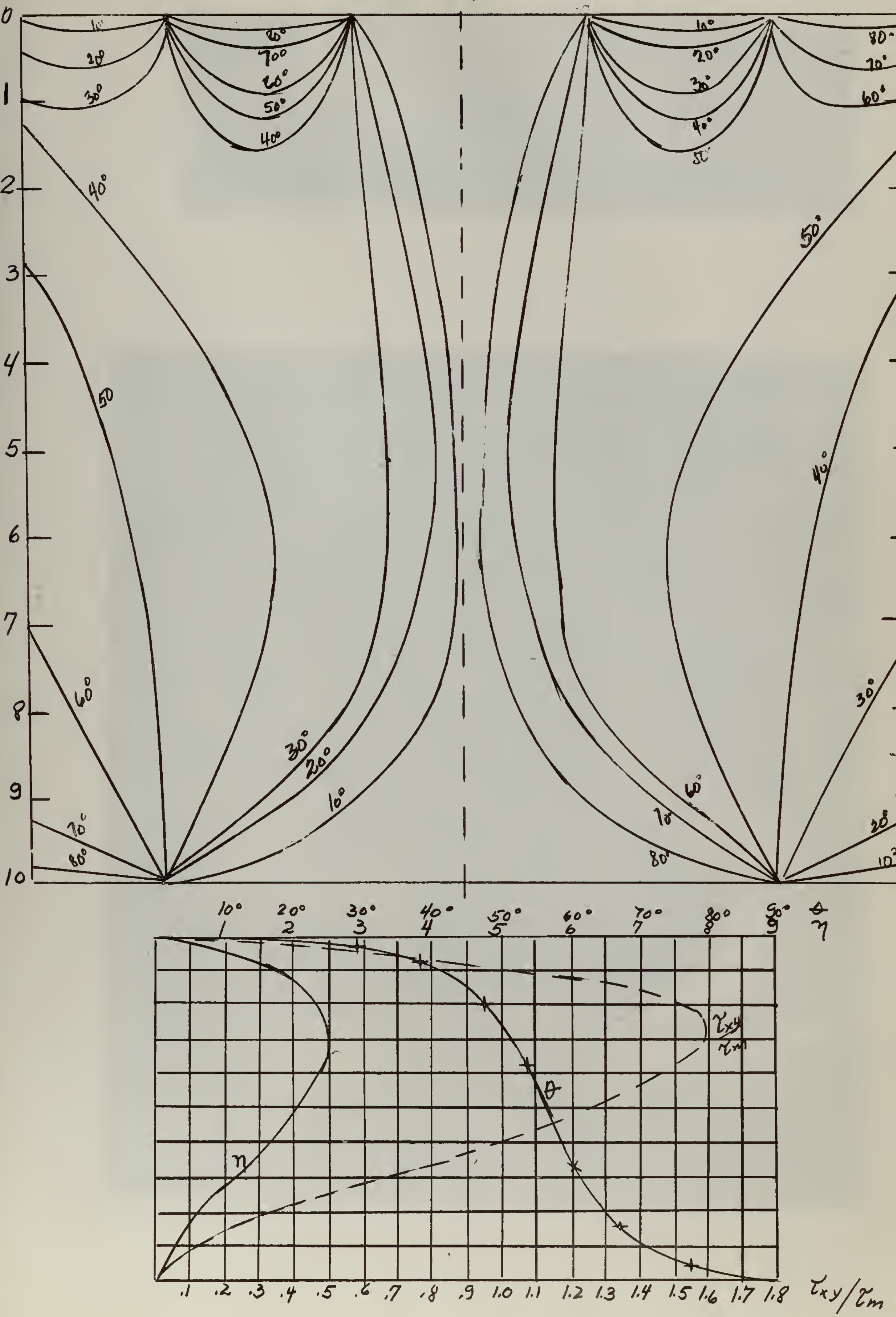

Figure XX

ASPECT RATIO 1:1

UNSTIFFENED

TABLE IV

Aspect Ratio 1:1 — 1 Stiffener

Load 500 psi.

Bottom Unsupported

Station	Order	θ	2θ	Sin 2θ	τ_{xy}	τ_{xy}/τ_m
0	0.2	0	0°	0	0	0
1	1.8	25°	50°	.7660	255	.91
2	2.4	34°	68°	.9271	412	1.47
3	2.4	41°	82°	.9902	440	1.57
4	2.2	45°	90°	1.00	407.4	1.45
5	1.8	49°	98°	.9902	330.	1.18
6	1.4	52°	104°	.9703	251	.90
7	1.2	56°	112°	.9271	206	.73
8	1.0	61°	122°	.8480	157	.57
9	0.6	69°	138°	.6691	74	.27
10	0	90°	180°	0	0	0

Bottom Supported

Station	Order	θ	2θ	Sin 2θ	τ_{xy}	τ_{xy}/τ_m
0	0	0	0°	0	0	0
1	1.4	27°	54°	.8090	209	.745
2	2.2	38°	76°	.9703	395	1.41
3	2.4	43°	86°	.9975	443	1.58
4	2.2	47°	94°	.9975	406	1.45
5	2	50°	100°	.9848	364	1.30
6	1.6	52°	104°	.9703	287	1.02
7	1.1	57°	114°	.9135	186	.66
8	0.9	62°	124°	.8290	138	.49
9	0.5	72°	144°	.5878	54	.09
10	0.2	90°	180	0	0	0

Figure XXI

Sketch of Isoclinics and Data for
AR 1:1 1 stiffener and unsupported

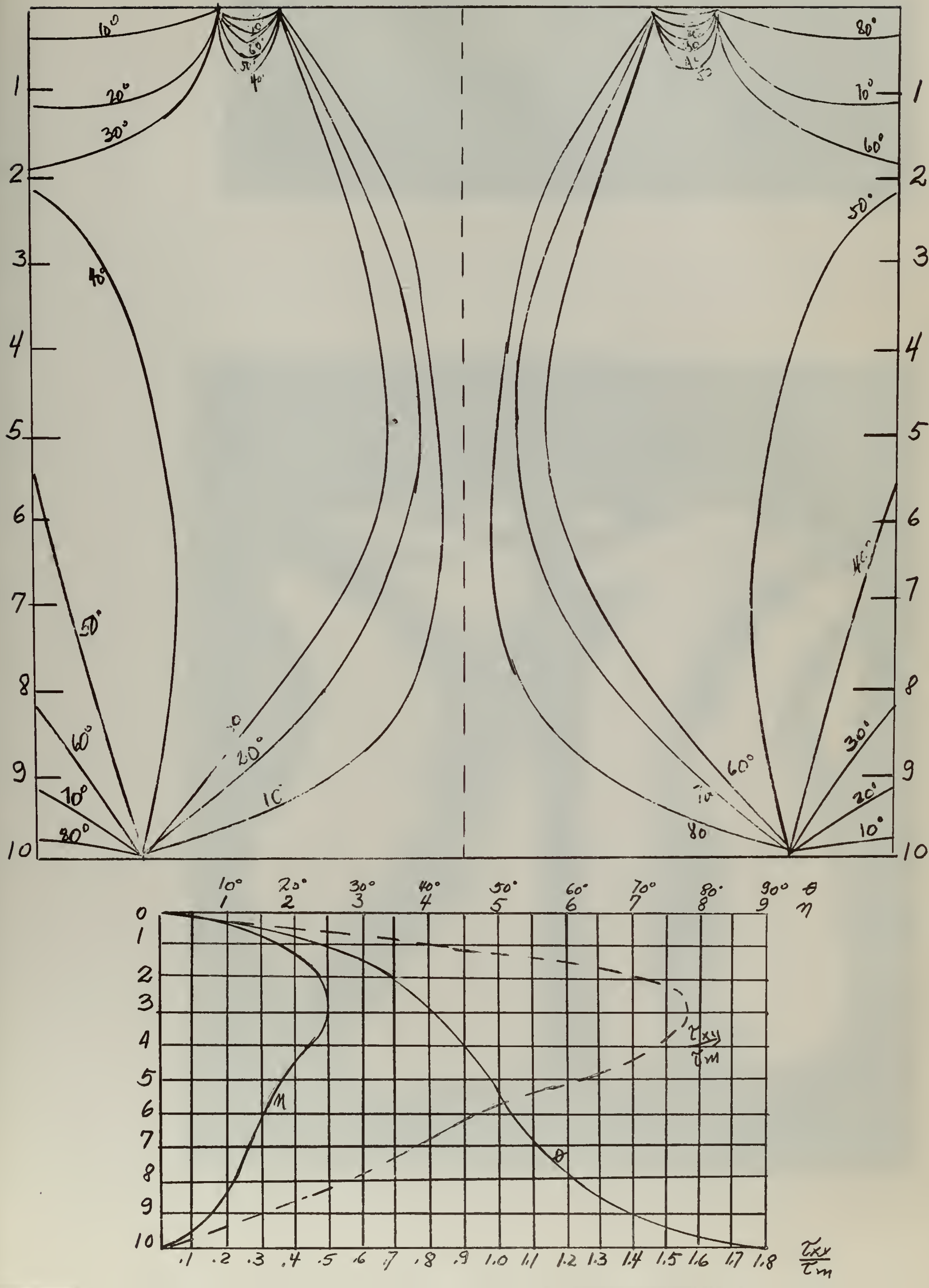

Figure XXII

ASPECT RATIO 1:1

1 STIFFENER

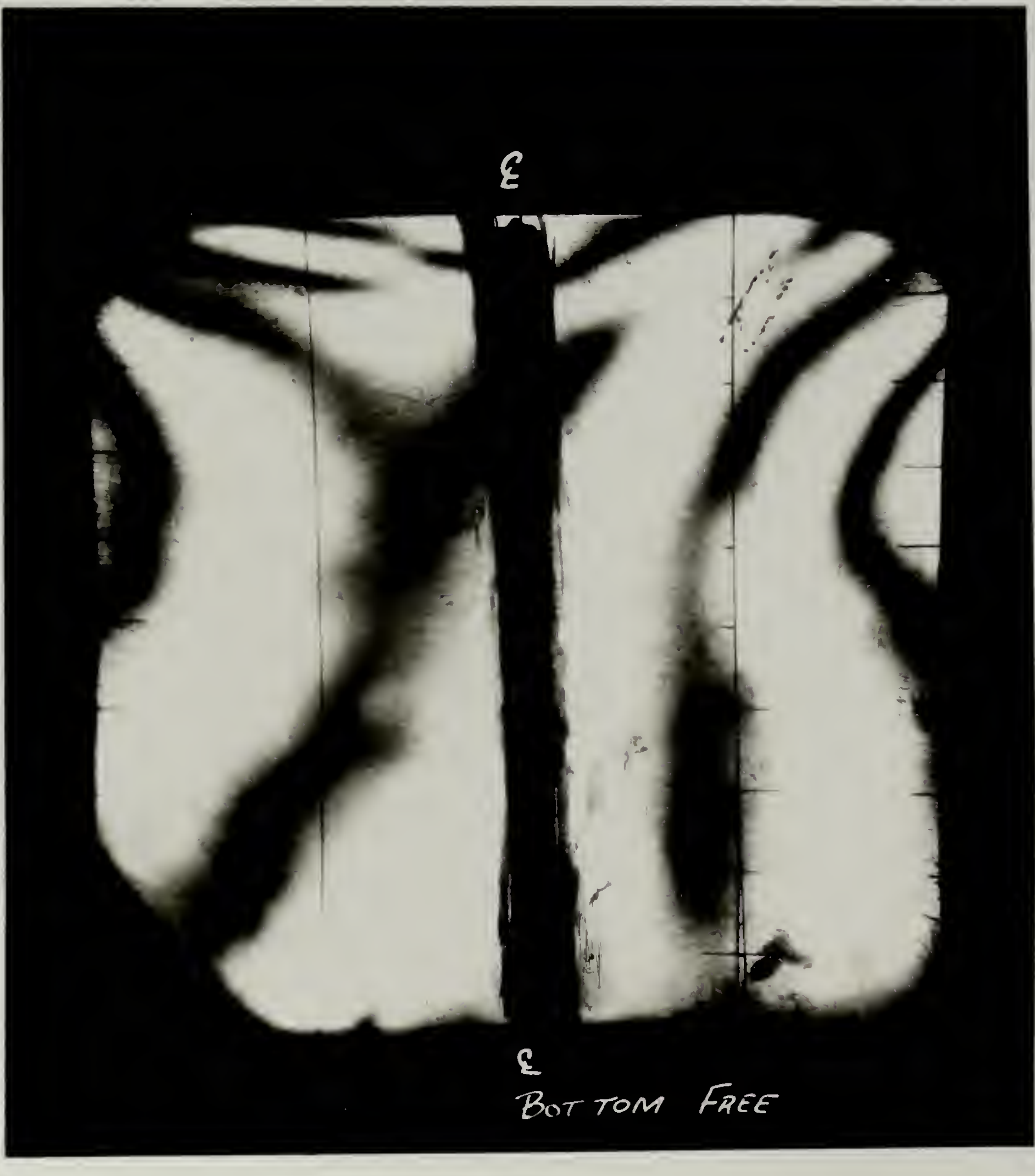

Figure XXIII

Sketch of Isoclinics and Data for AR 1:1
1 stiffener and supported

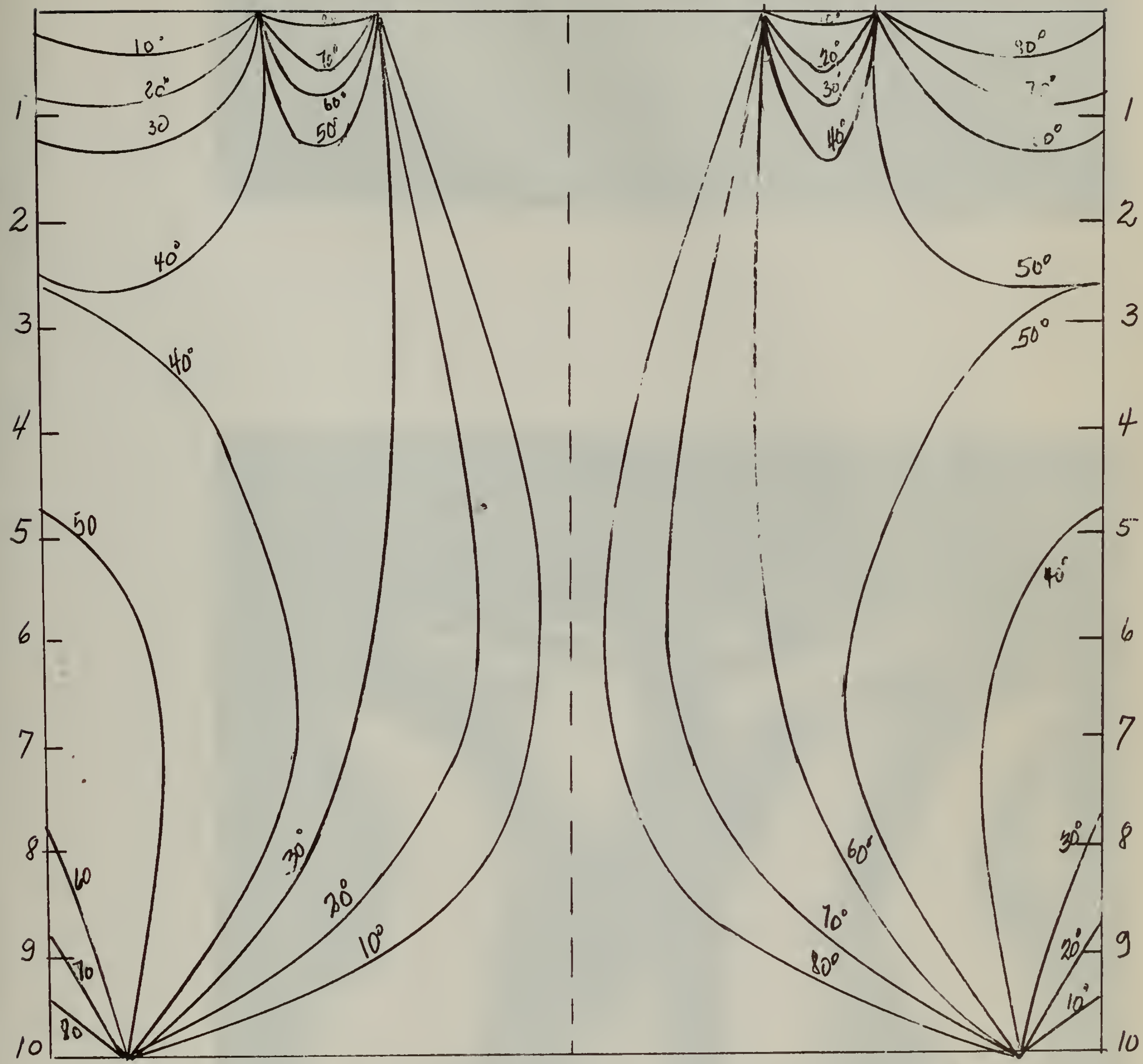

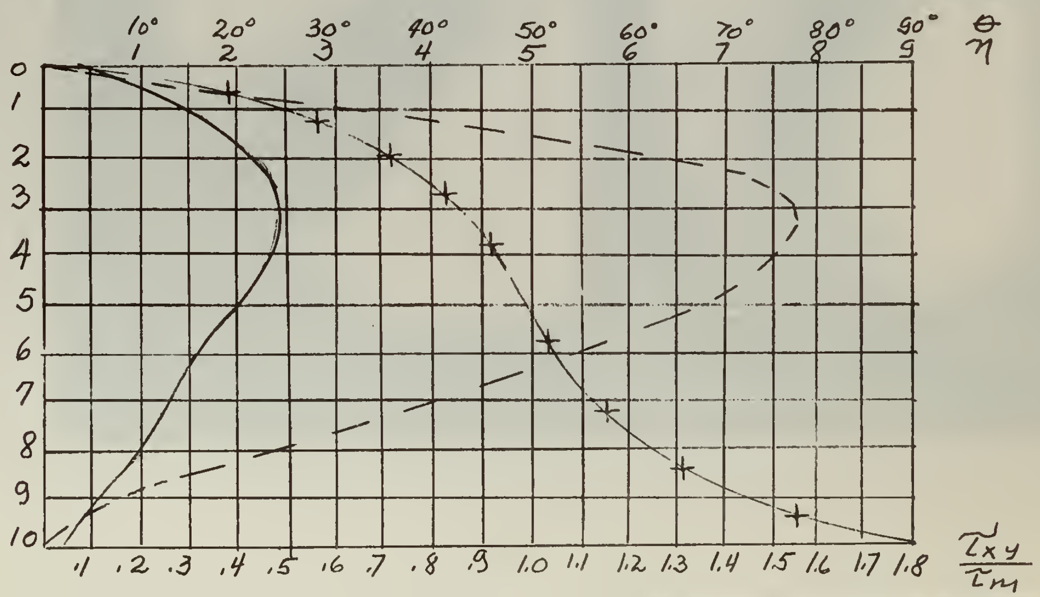

Figure XXIV

ASPECT RATIO 1:1

1 STIFFENER

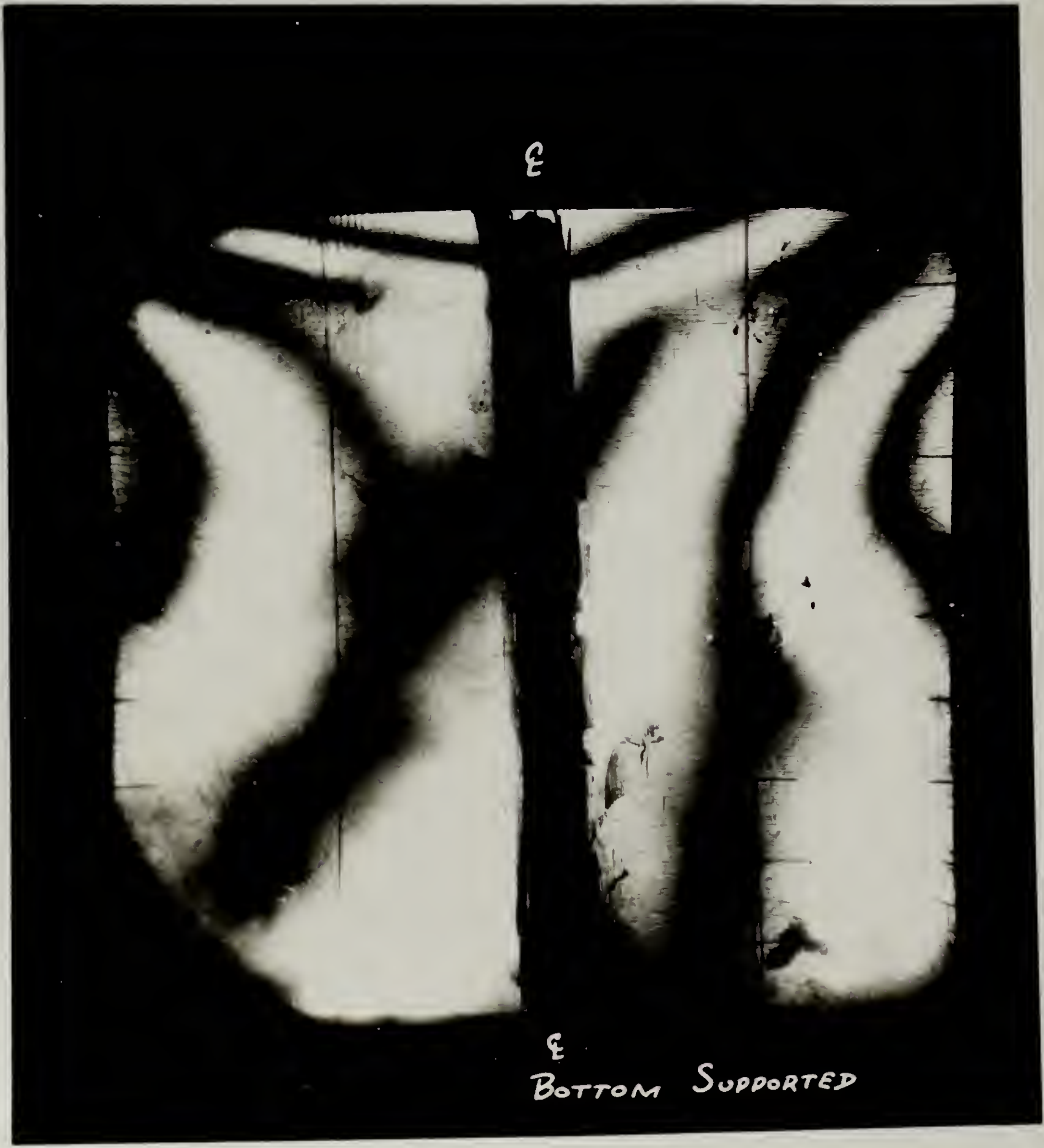

TABLE V

Aspect Ratio 1:1 2 Stiffeners

Load 500 psi.

Bottom Unsupported

Station	Order	θ	2θ	Sin 2θ	τ_{xy}	τ_{xy}/τ_m
0	1.3	0^o	0^o	0	0	0
1	2.0	32^o	64^o	.8987	332	1.17
2	2.5	40^o	80^o	.9448	437	1.56
3	2.4	43^o	86^o	.9975	443	1.58
4	2.2	47^o	94^o	.9975	406	1.45
5	2.0	50^o	100^o	.9848	364	1.30
6	1.7	54^o	108^o	.9110	286	1.02
7	1.4	57^o	114^o	.9135	236	.84
8	1.1	60^o	120^o	.8660	176	.63
9	.6	68^o	136^o	.6946	77	.27
10	0	90^o	180^o	0	0	0

Bottom Supported

Station	Order	θ	2θ	Sin 2θ	τ_{xy}	τ_{xy}/τ_m
0	1.4	0^o	0^o	0	0	0
1	1.9	37^o	74^o	.9612	338	1.21
2	2.4	46^o	92^o	.9993	444	1.58
3	2.5	50^o	100^o	.9848	456	1.63
4	2.1	52^o	104^o	.9703	377	1.35
5	1.7	54^o	108^o	.9510	299	1.07
6	1.3	57^o	114^o	.9135	220	.79
7	1.0	60^o	120^o	.8660	160	.57
8	0.8	64^o	128^o	.7880	116	.41
9	0.5	70^o	140^o	.6427	60	.21
10	0	90^o	180^o	0	0	0

Figure XXV

Sketch of Isoclinics and Data for AR 1:1
2 stiffeners and unsupported

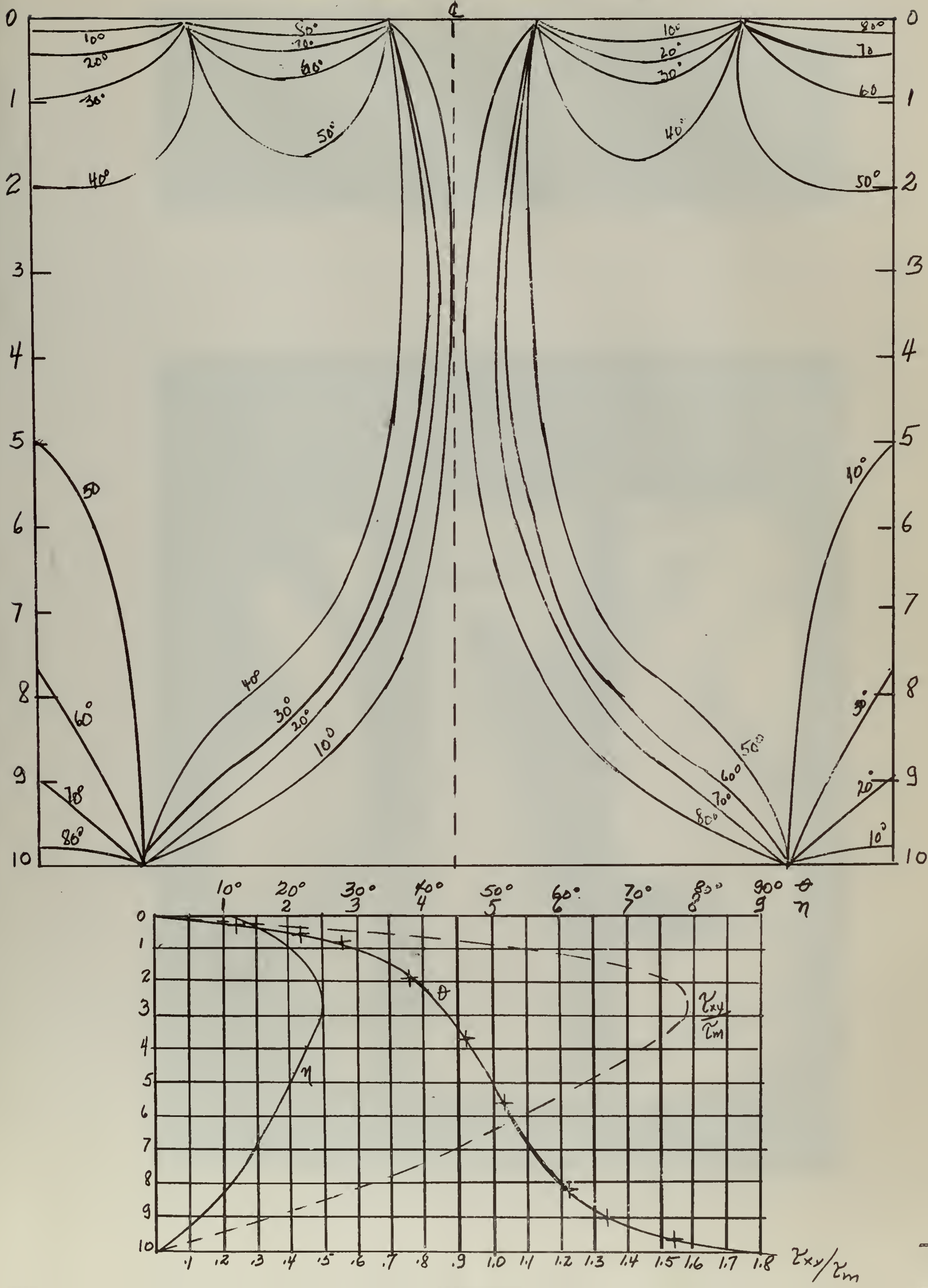

Figure XXVI

Aspect Ratio 1:1

2 Stiffeners

Figure XXVII

Sketch of Isoclinics and Data for AR 1:1
2 stiffeners and supported

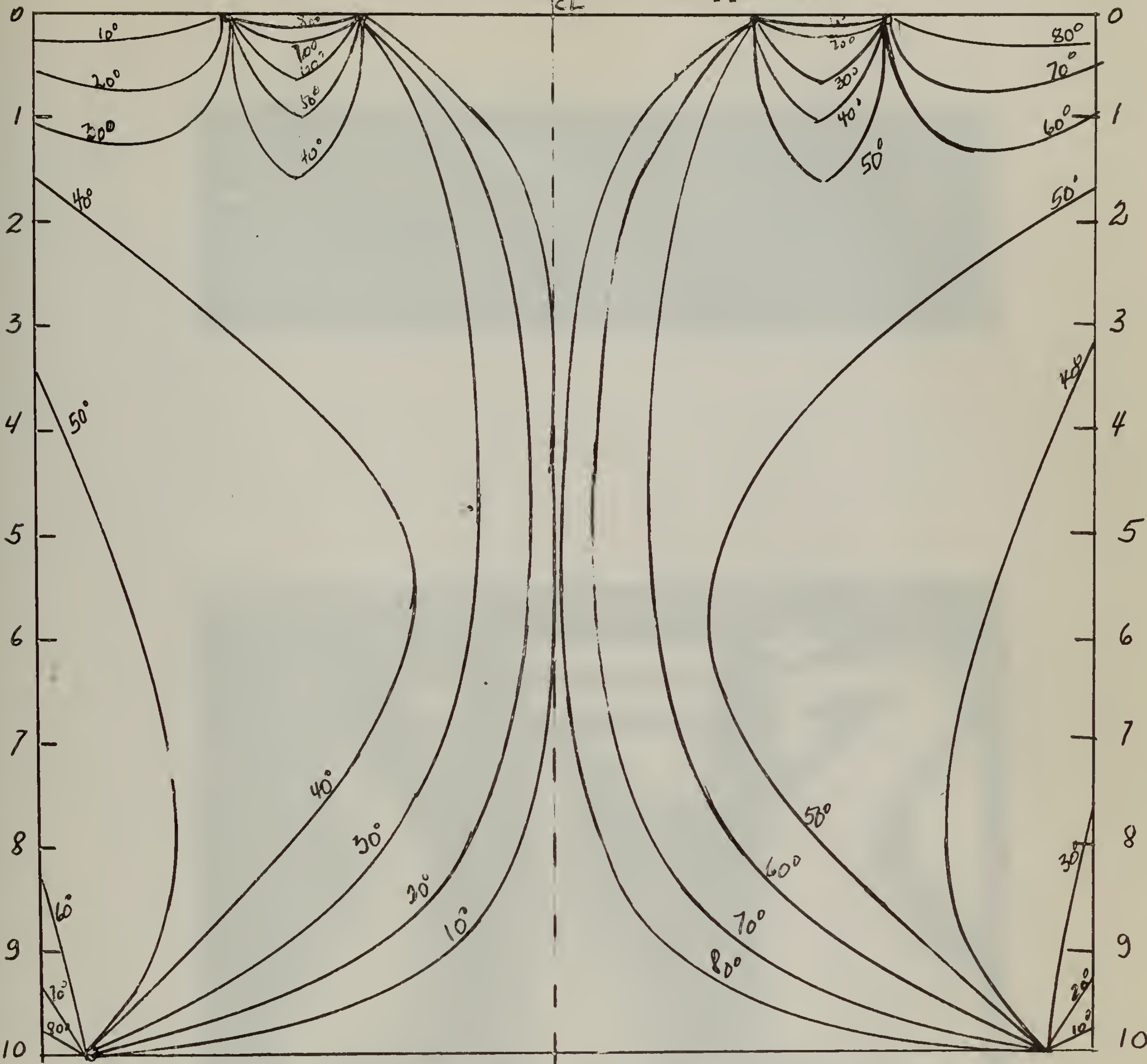

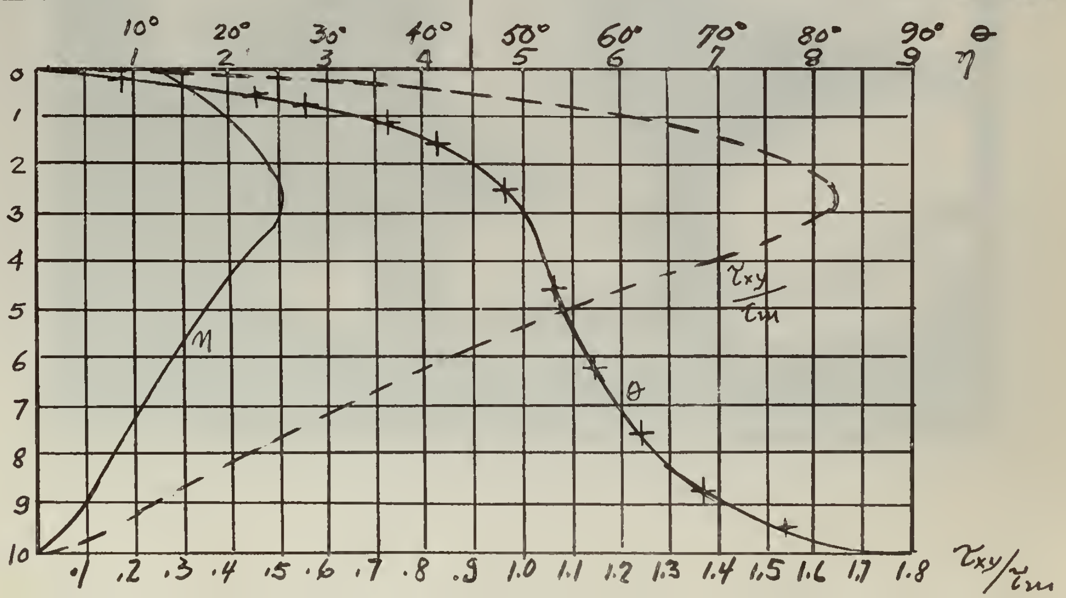

Figure XXVIII

ASPECT RATIO 1:1

2 STIFFENERS

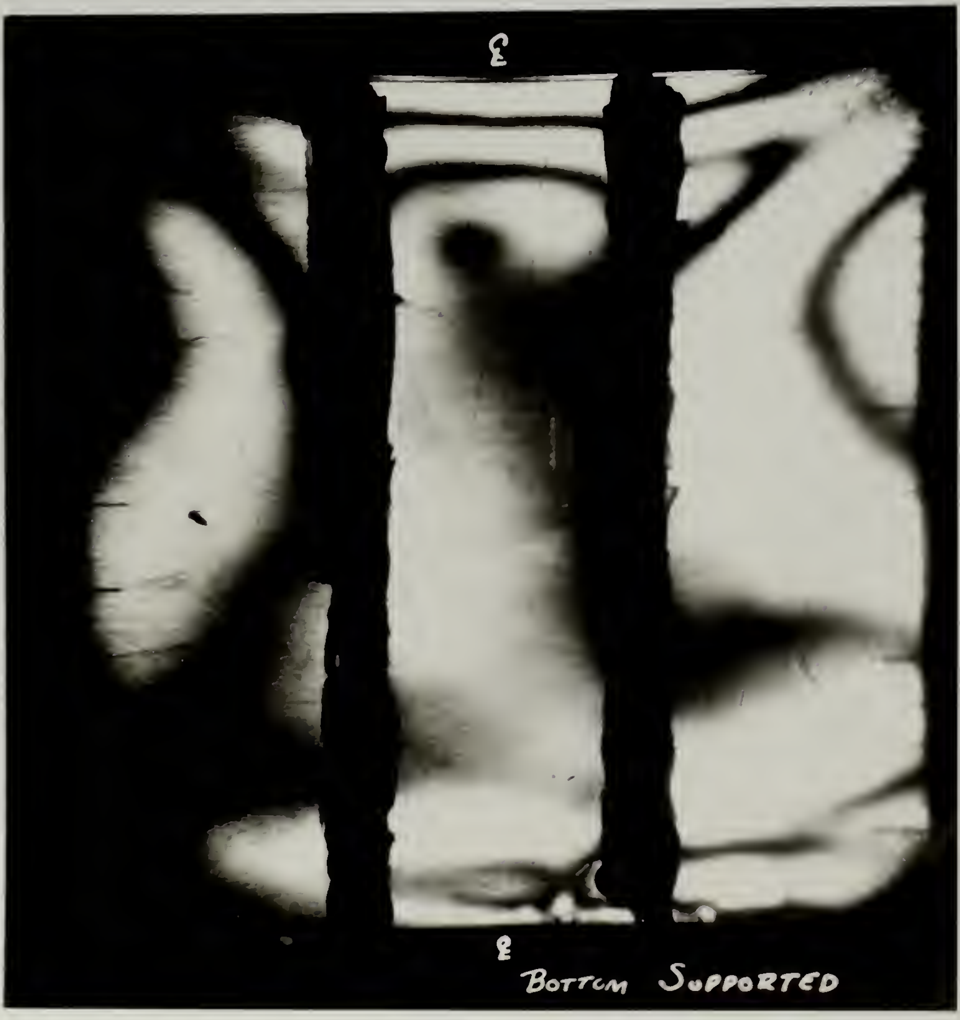

TABLE VI

Aspect Ratio 1:1 — 3 Stiffeners

Load 500 psi.

Bottom Unsupported

Station	Order	θ	2θ	Sin 2θ	τ_{xy}	τ_{xy}/τ_m
0	0	0°	0°	0	0	0
1	1.3	20°	40°	.6428	154	.55
2	2.0	33°	66°	.9135	338	1.20
3	2.2	40°	80°	.9848	401	1.43
4	2.1	43°	86°	.9975	390	1.39
5	1.7	45°	90°	1.000	314	1.12
6	1.5	47°	94°	.9975	277	.99
7	1.3	51°	102°	.9781	235	.84
8	1.1	58°	116°	.8987	183	.65
9	0.9	67°	134°	.7193	119	.43
10	0.8	90°	180°	0	0	0

Bottom Supported

Station	Order	θ	2θ	Sin 2θ	τ_{xy}	τ_{xy}/τ_m
0	0	0°	0°	0	0	0
1	1.7	18°	36°	.5878	185	.66
2	2.1	31°	62°	.8829	343	1.23
3	2.2	40°	80°	.9448	384	1.37
4	2.1	46°	92°	.9993	388	1.38
5	1.9	50°	100°	.9848	346	1.23
6	1.7	54°	108°	.9510	299	1.07
7	1.4	60°	120°	.8660	224	.80
8	1.1	64°	128°	.7880	160	.57
9	0.8	72°	144°	.5878	87	.31
10	0.4	90°	180°	0	0	0

Figure XXIX

Sketch of Isoclinics and Data for AR 1:1
3 stiffeners and unsupported

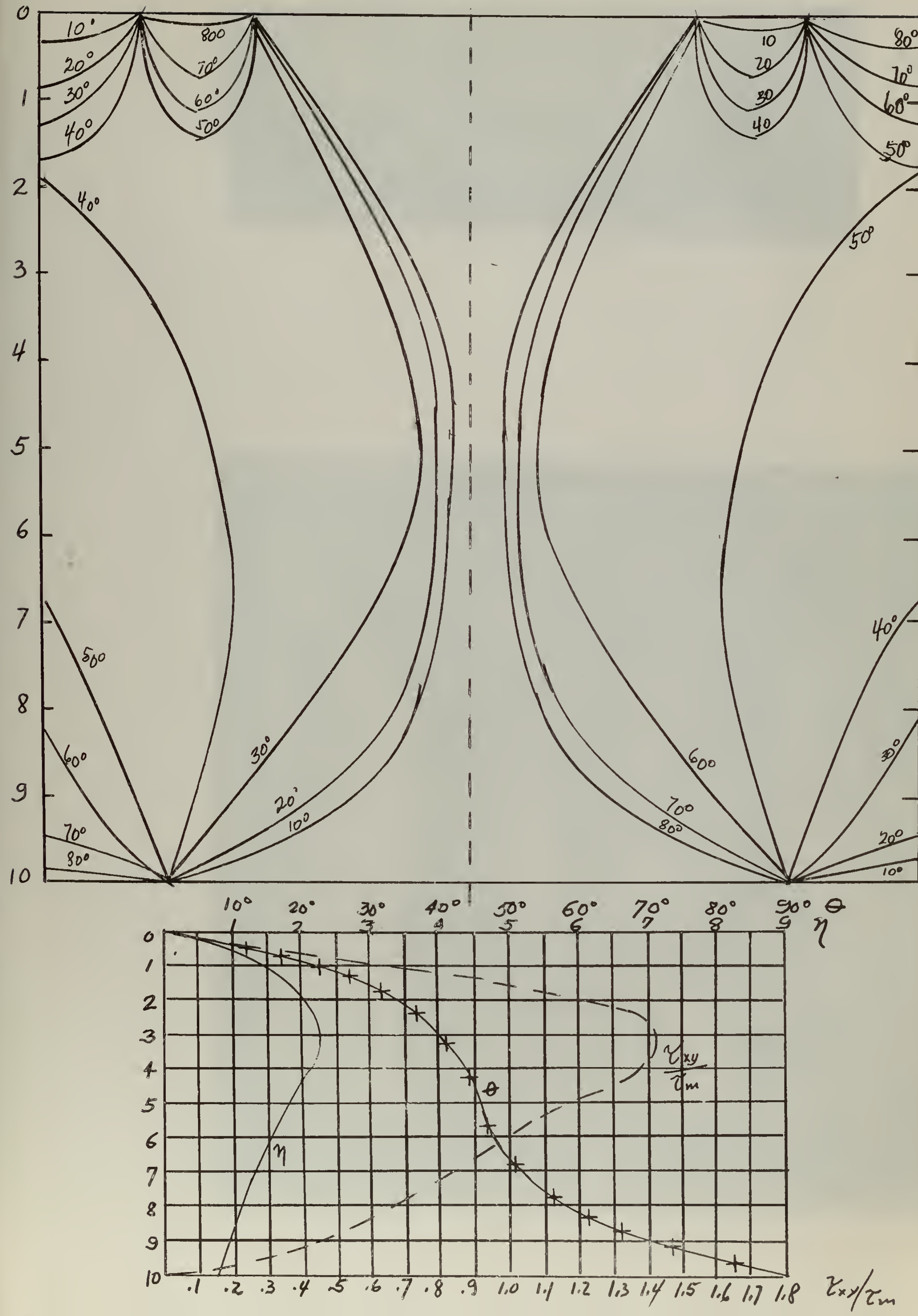

Figure xxx

ASPECT RATIO 1:1

3 STIFFENERS

Figure XXXI

Sketch of Isoclinics and Data for AR 1:1
3 stiffeners and supported

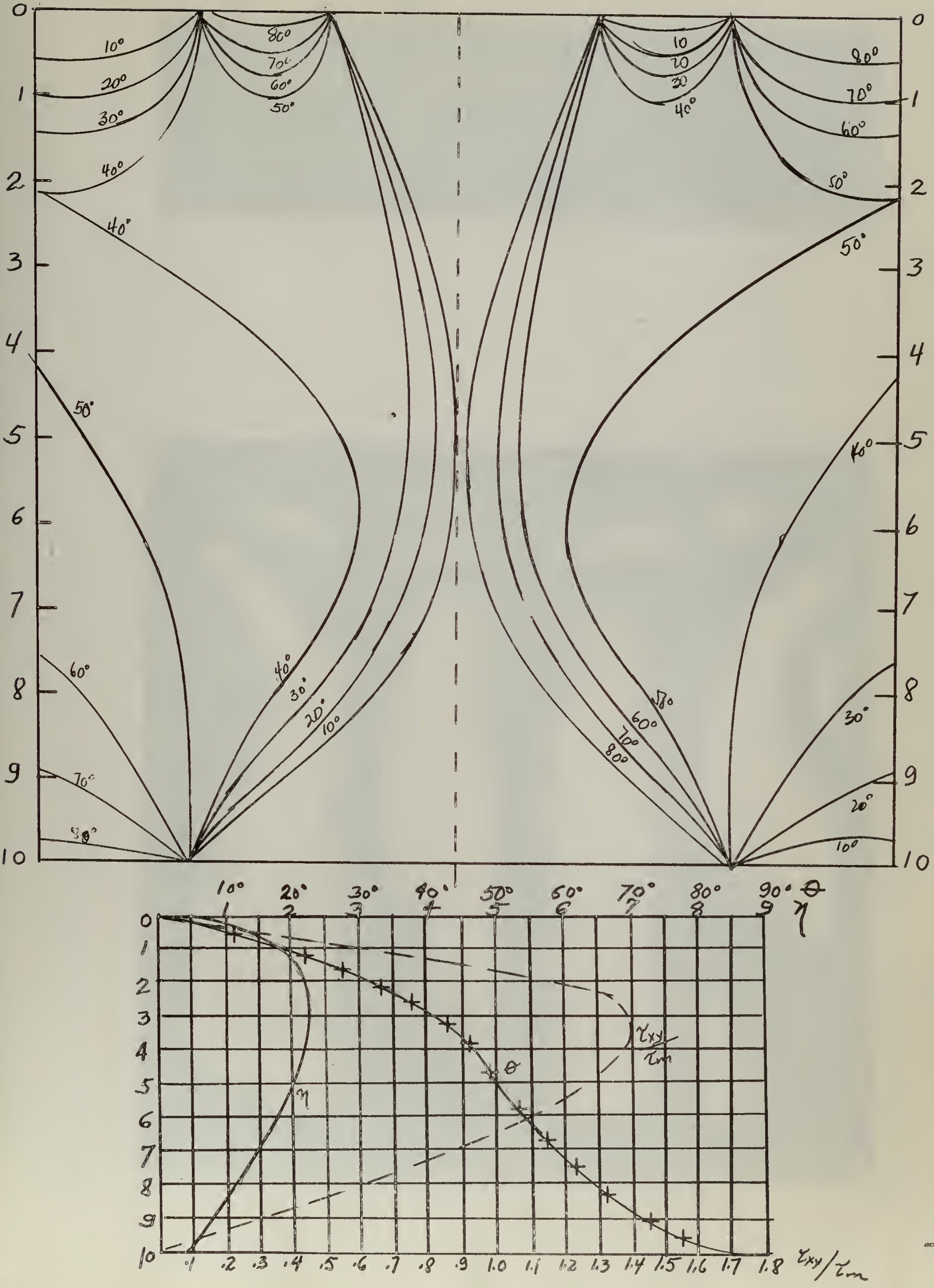

Figure XXXII

ASPECT RATIO 1:1

3 STIFFENERS

TABLE VII

Aspect Ratio 2:1 | 2 Stiffeners

Load 500 psi

Bottom Unsupported

Station	Order	θ	2θ	Sin 2θ	τ_{xy}	τ_{xy}/τ_m
0	2.1	0°	0°	0	0	0.0
1	3.10	38°	76°	.97030	.557	.995
2	3.8	43°	86°	.99756	.702	1.25
3	4.3	45°	90°	1.000	.796	1.425
4	4.4	47°	94°	.99756	.812	1.45
5	4.4	49°	98°	.99027	.807	1.44
6	4.0	51°	102°	.97815	.724	1.29
7	3.4	53°	106°	.97437	.613	1.10
8	2.6	59°	118°	.88295	.425	.76
9	1.8	70°	140°	.64279	.214	.382
10	1.0	90°	180°	0	0	0.0
Bottom Supported						
0	1.6	0°	0°	0.0	0.0	0.0
1	2.4	37°	74°	.96126	427	.76
2	2.9	44°	88°	.99939	536	.956
3	3.1	47°	94°	.99756	572	1.02
4	3.1	49°	98°	.99027	568	1.01
5	2.9	52°	104°	.9703	521	.93
6	2.5	55°	110°	.93969	435	.78
7	2.1	57°	114°	.91355	355	.63
8	1.7	61°	122°	.84805	267	.48
9	1.3	70°	140°	.64279	154	.275
10	0.9	90°	180°	0.0	0.0	0.0

Figure XXXIII

Sketch of Isoclinics and Data for AR 2:1
2 stiffeners and unsupported

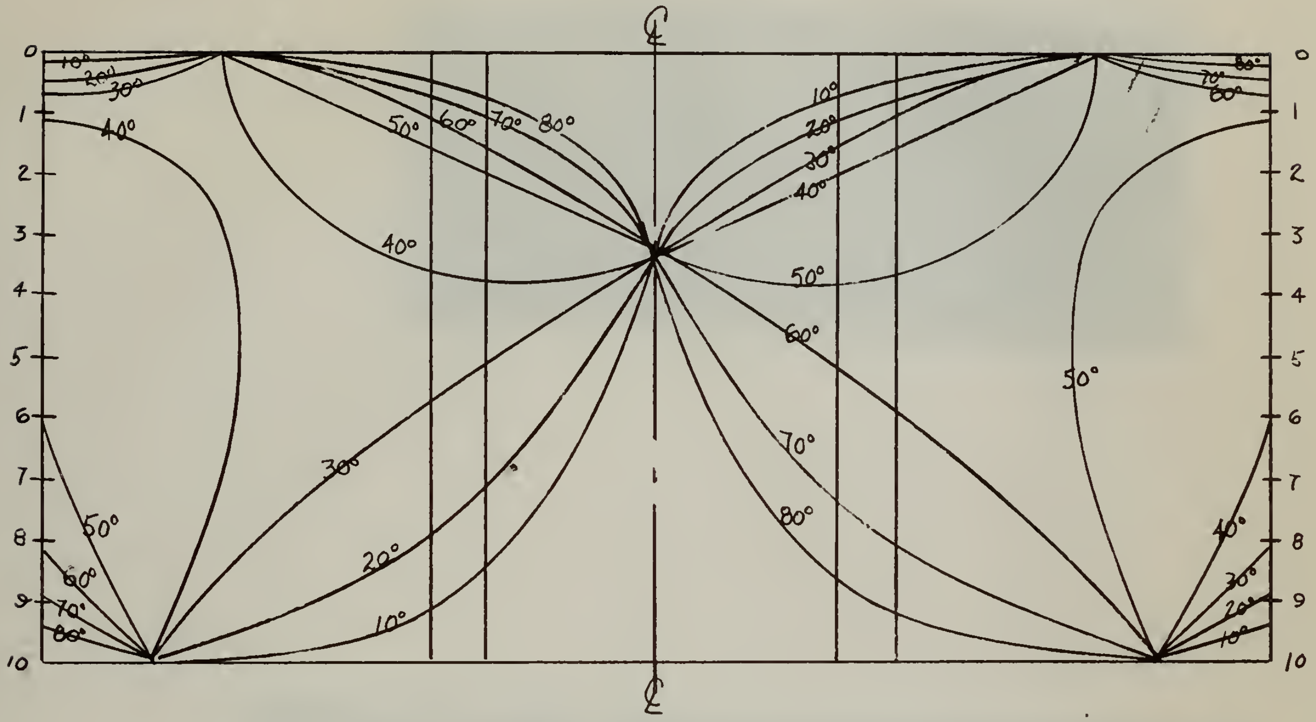

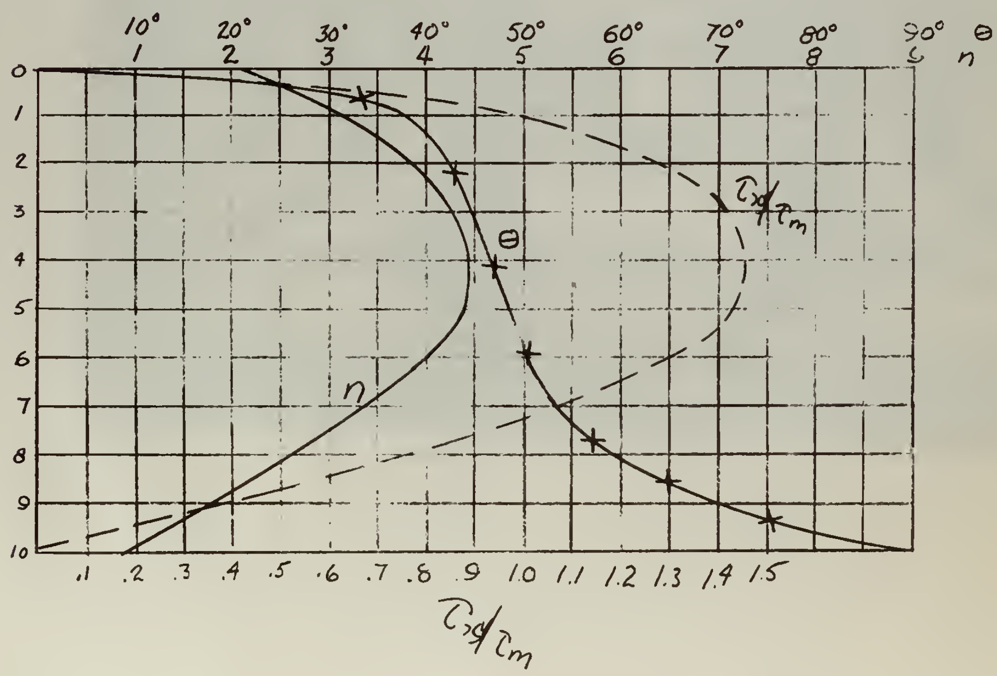

Figure XXXIV

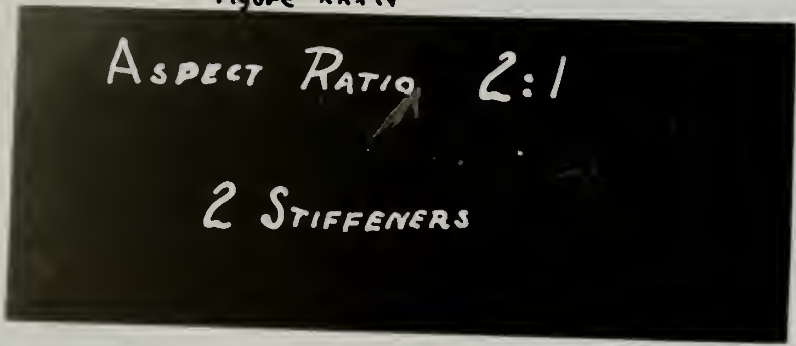

Figure XXXV

Sketch of Isoclinics and Data for AR 2:1
2 stiffeners and supported

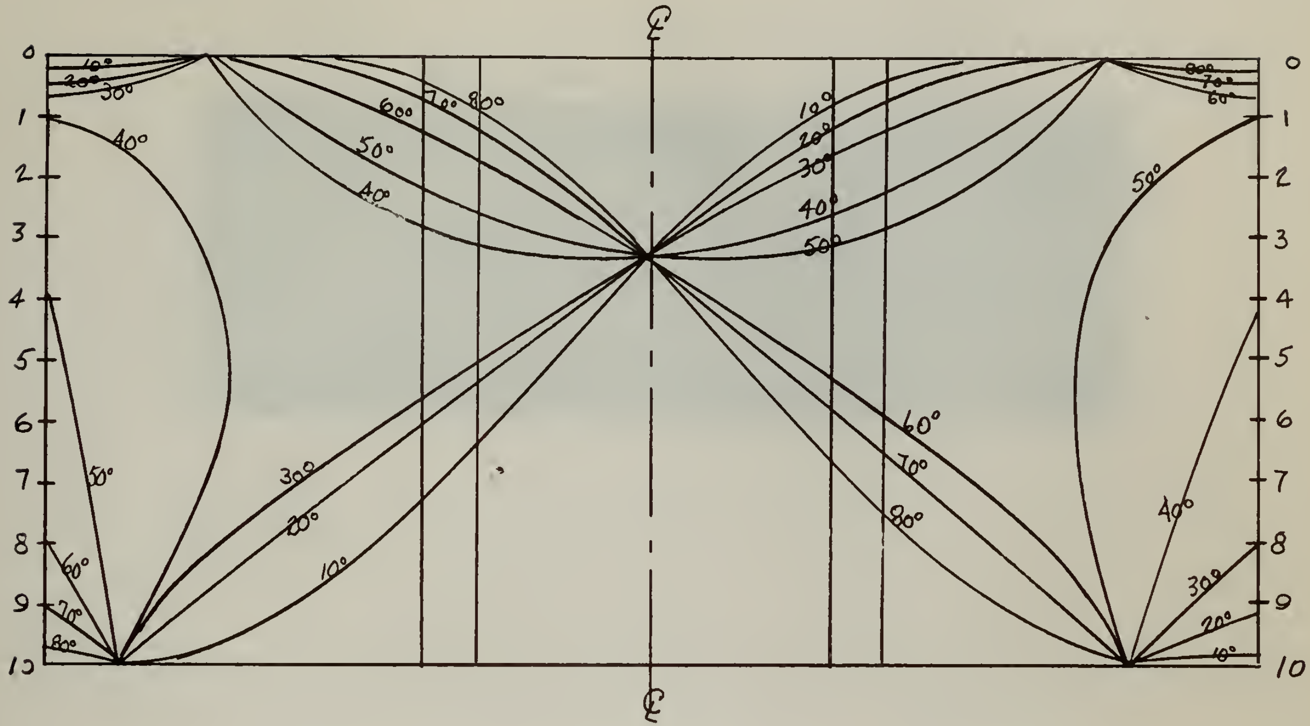

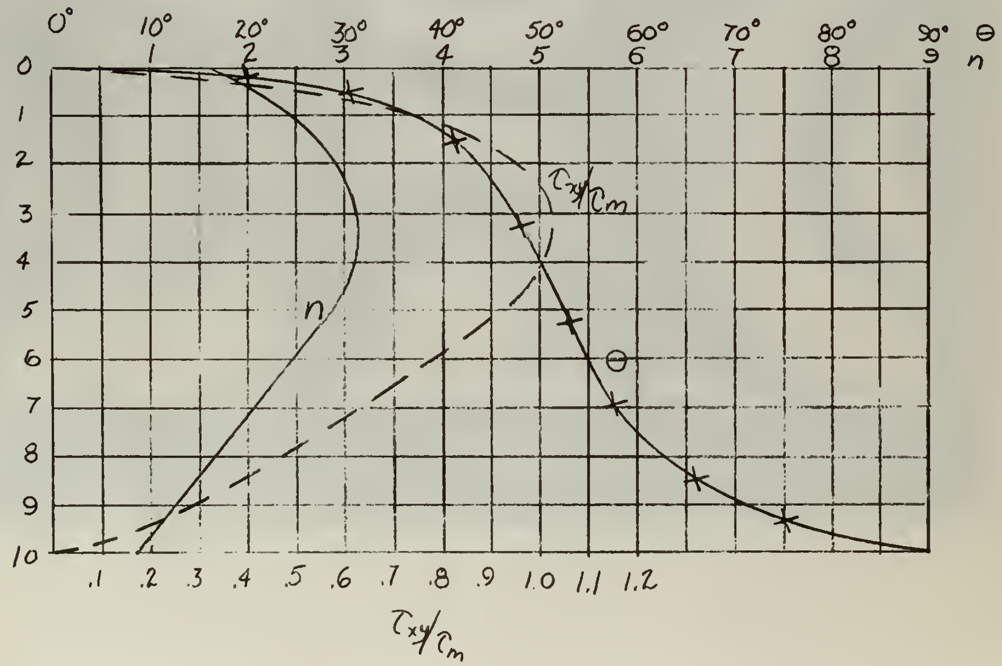

Figure XXXVI

ASPECT RATIO 2:1

2 STIFFENERS

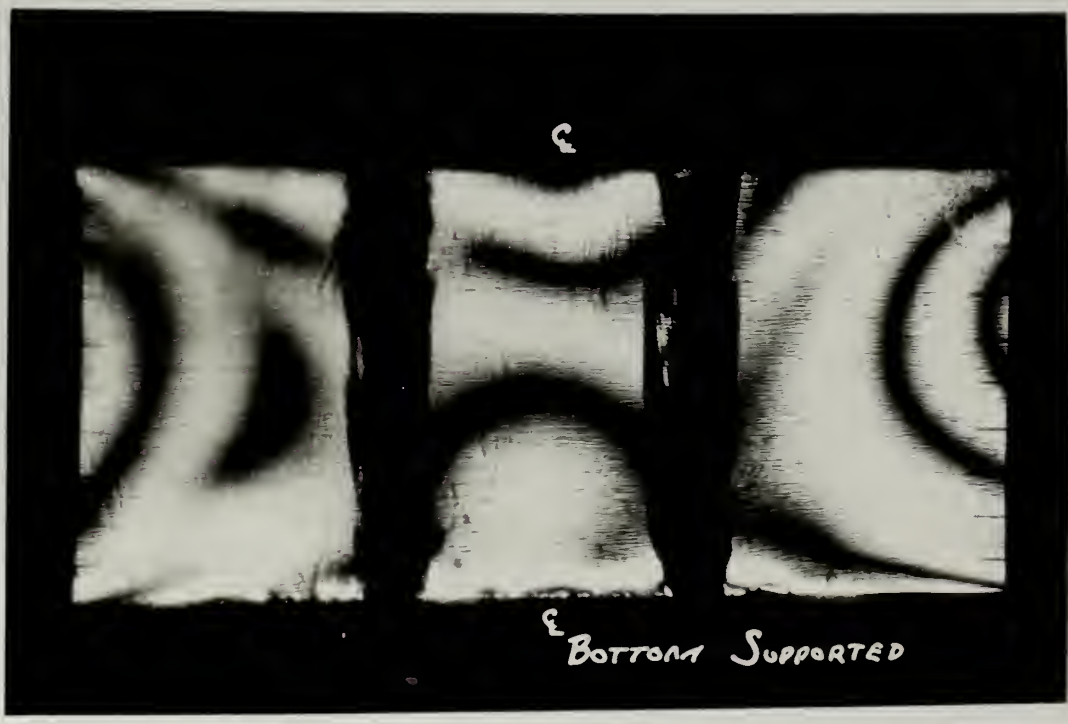

TABLE VIII

Aspect Ratio 2:1

3 Stiffeners

Load 500 psi.

Bottom Unsupported

Station	Order	θ	2θ	Sin 2θ	τ_{xy}	τ_{xy}/τ_m
0	0.3	0°	0°	0.0	0.0	0.0
1	1.7	19°	38°	.61566	193	.345
2	3.0	32°	64°	.89879	499	.89
3	3.9	40°	80°	.9848	711	1.27
4	4.2	43°	86°	.99756	776	1.39
5	4.1	47°	94°	.99756	757	1.35
6	4.0	50°	100°	.9848	729	1.30
7	3.3	54°	108°	.95160	581	1.04
8	2.5	60°	120°	.8660	401	.716
9	1.4	70°	140°	.46279	120	.215
10	0.4	90°	180°	0.0	0	0.0

Bottom Supported

Station	Order	θ	2θ	Sin 2θ	τ_{xy}	τ_{xy}/τ_m
0	1.5	0°	0°	0.0	0	0.0
1	2.7	15°	30°	.5000	250	.446
2	3.1	29°	58°	.84805	487	.87
3	3.4	39°	78°	.97815	616	1.10
4	3.4	45°	90°	1.00	629	1.12
5	3.4	50°	100°	.9848	620	1.11
6	3.2	53°	106°	.97437	577	1.03
7	2.9	57°	114°	.91355	490	.878
8	2.5	63°	126°	.8090	374	.67
9	2.0	74°	148°	.52992	196	.35
10	1.3	90°	180°	0.0	0	0.0

Figure XXXVII

Sketch of Isoclinics and Data for AR 2:1
3 stiffeners and unsupported

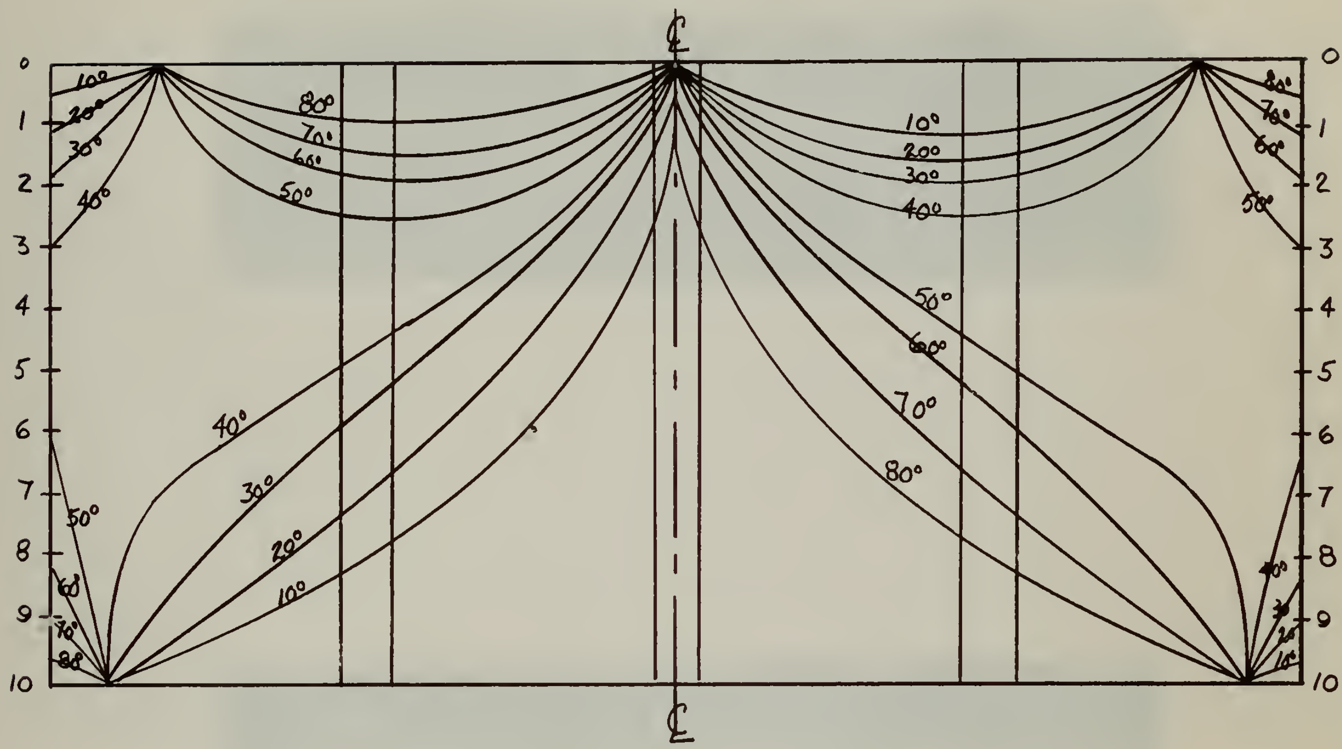

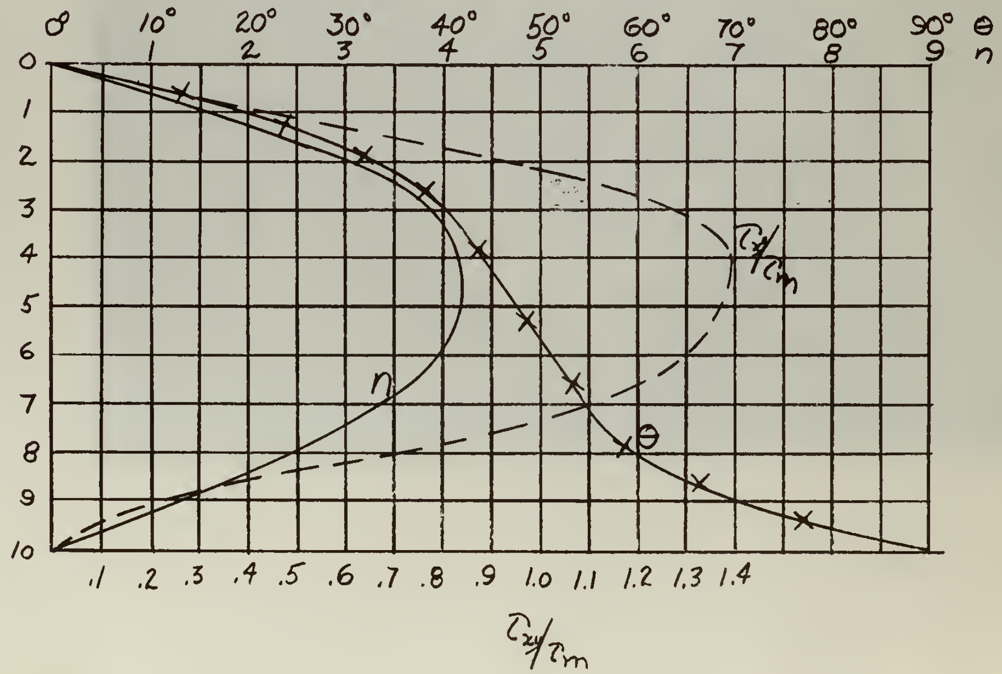

Figure XXXVIII

ASPECT RATIO 2:1

3 STIFFENERS

Figure XXXIX

Sketch of Isoclinics and Data for AR 2:1
3 stiffeners and supported

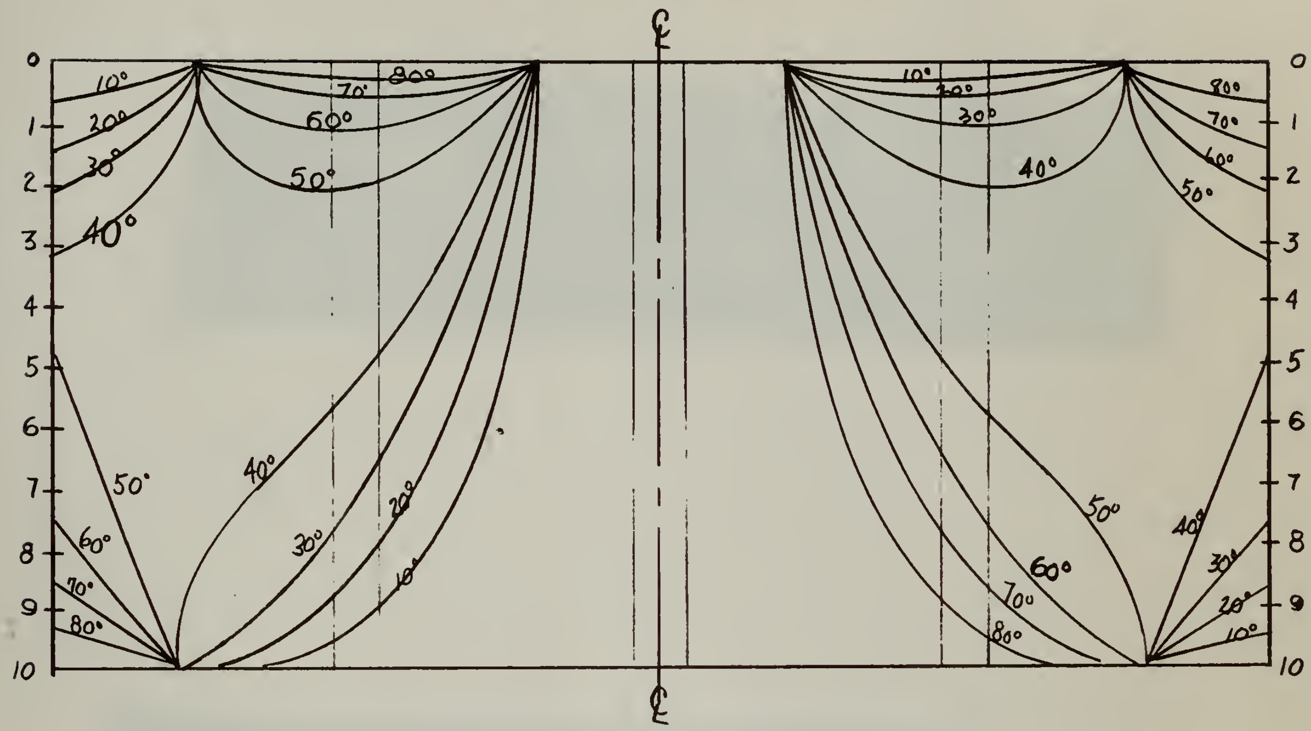

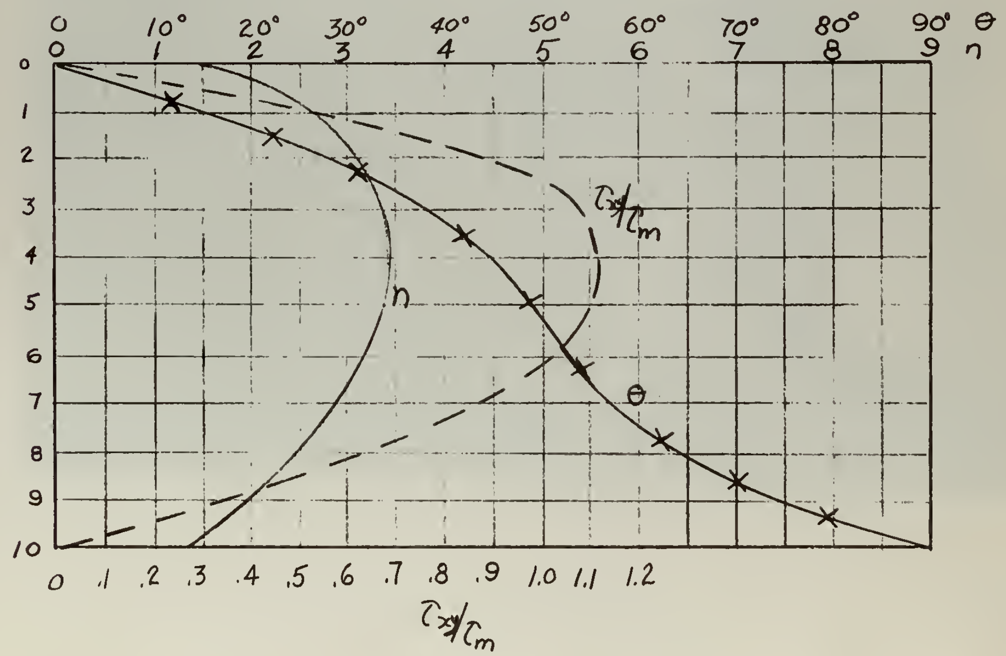

Figure XL

ASPECT RATIO 2:1

3 STIFFENERS

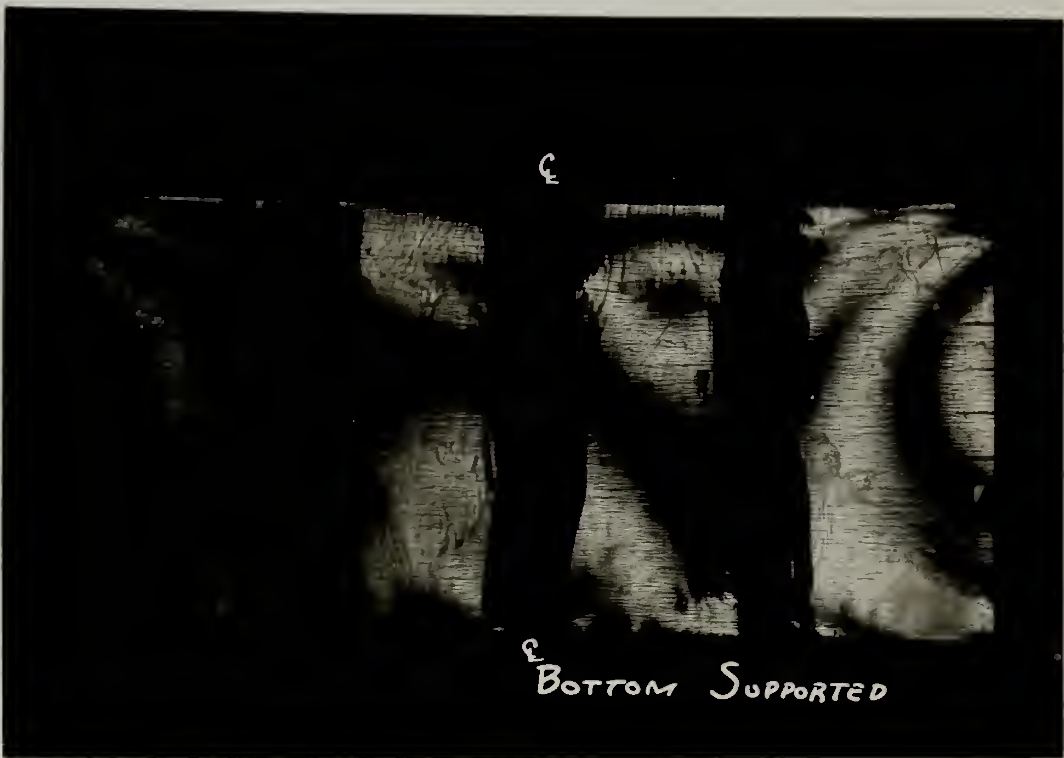

TABLE IX

Aspect Ratio 3:1 — 2 Stiffeners

Load 450 psi.

Bottom Unsupported

Station	Order	θ	2θ	Sin 2θ	τ_{xy}	τ_{xy}/τ_{n}
0	2.2	0°	0°	0	0.0	0.0
1	3.0	14°	28°	.4694	243	.332
2	4.3	25°	50°	.7660	568.3	.777
3	4.8	33°	66°	.9135	756.6	1.03
4	5.1	40°	80°	.9848	867	1.185
5	5.1	46°	92°	.9993	879	1.20
6	4.9	52°	104°	.9703	820	1.12
7	4.5	60°	120°	.8660	673	.92
8	3.9	69°	138°	.6691	450	.615
9	3.0	80°	160°	.3420	178	.243
10	2.1	90°	180°	0	0.0	0.0

Bottom Supported

Station	Order	θ	2θ	Sin 2θ	τ_{xy}	τ_{xy}/τ_{n}
0	2.4	0°	0°	0	0.0	0.0
1	3.1	15°	30°	.50	267	.355
2	3.9	28°	56°	.829	557	.76
3	4.5	38°	76°	.9703	752	1.03
4	4.8	46°	92°	.9993	826	1.13
5	4.6	52°	104°	.9703	769	1.05
6	4.2	58°	116°	.8987	650	.89
7	3.7	63°	126°	.8090	516	.706
8	3.2	71°	142°	.6156	340	.465
9	2.9	80°	160°	.3420	171	.234
10	2.7	90°	180°	0	0.0	0.0

Figure XLI

Sketch of Isoclinics and Data for AR 3:1
2 stiffeners and unsupported

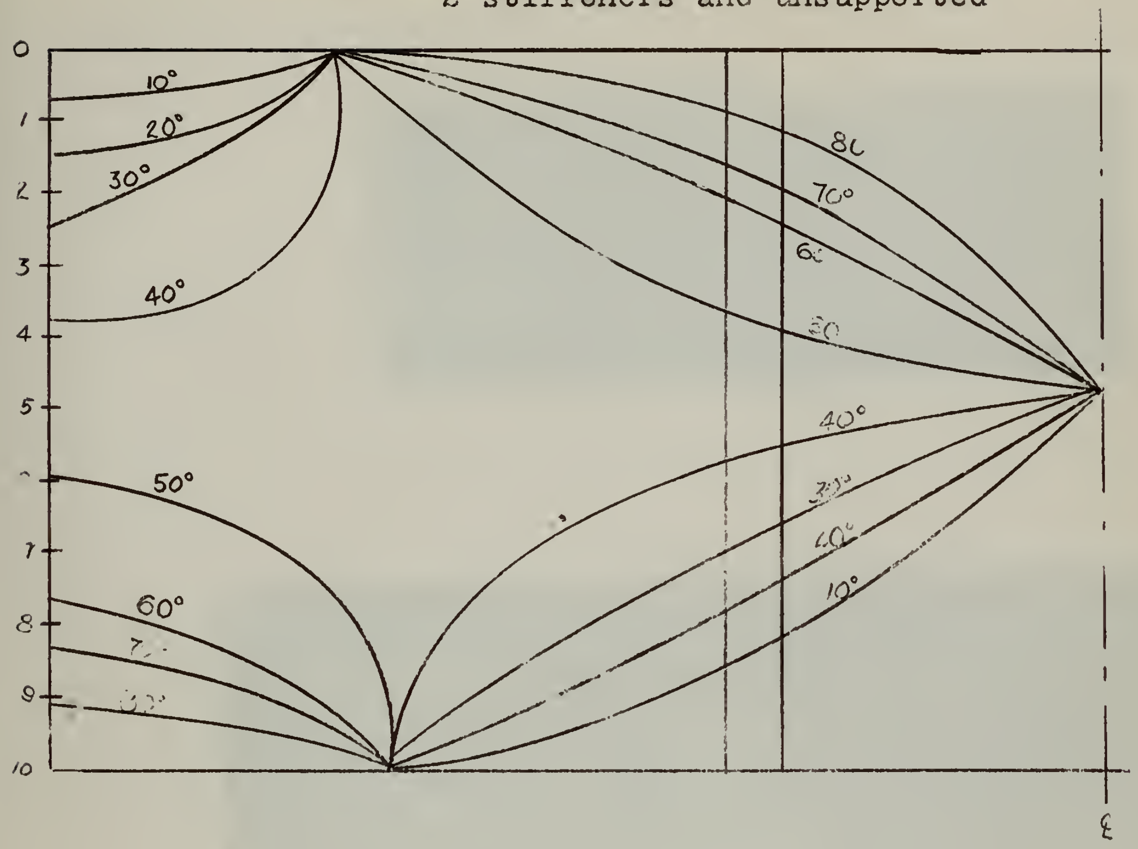

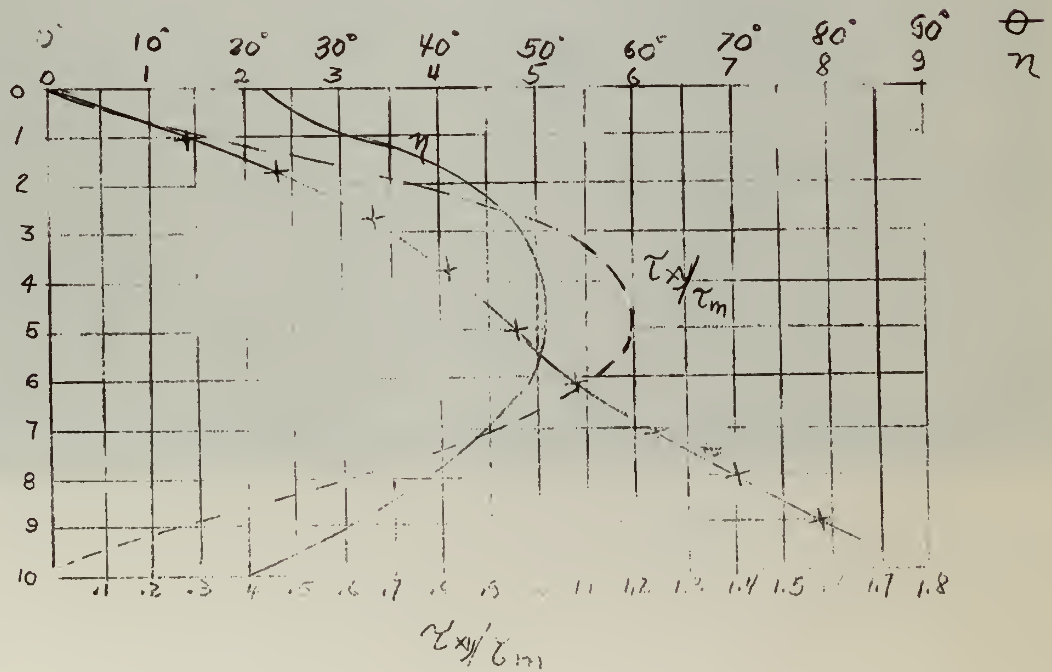

Figure XLII

ASPECT RATIO 3:1

2 STIFFENERS

Figure XLIII

Sketch of Isoclinics and Data for AR 3:1
2 stiffeners and supported

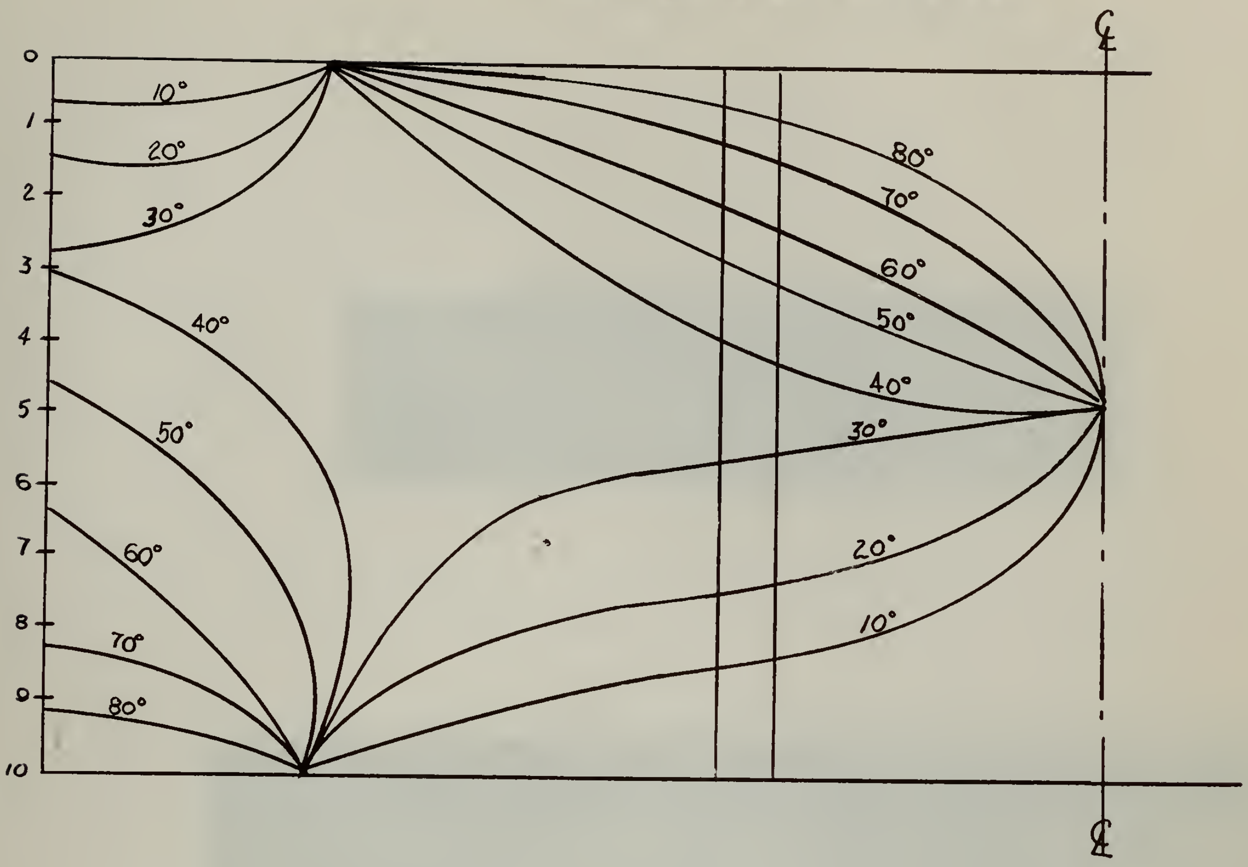

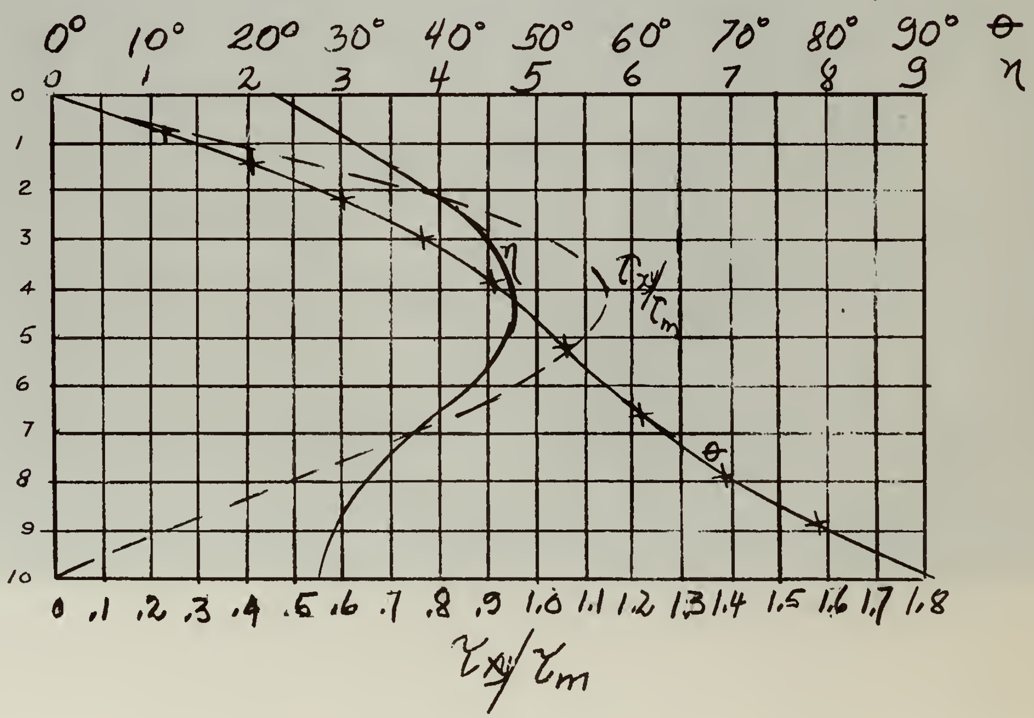

Figure XLIV

ASPECT RATIO 3:1

2 STIFFENERS

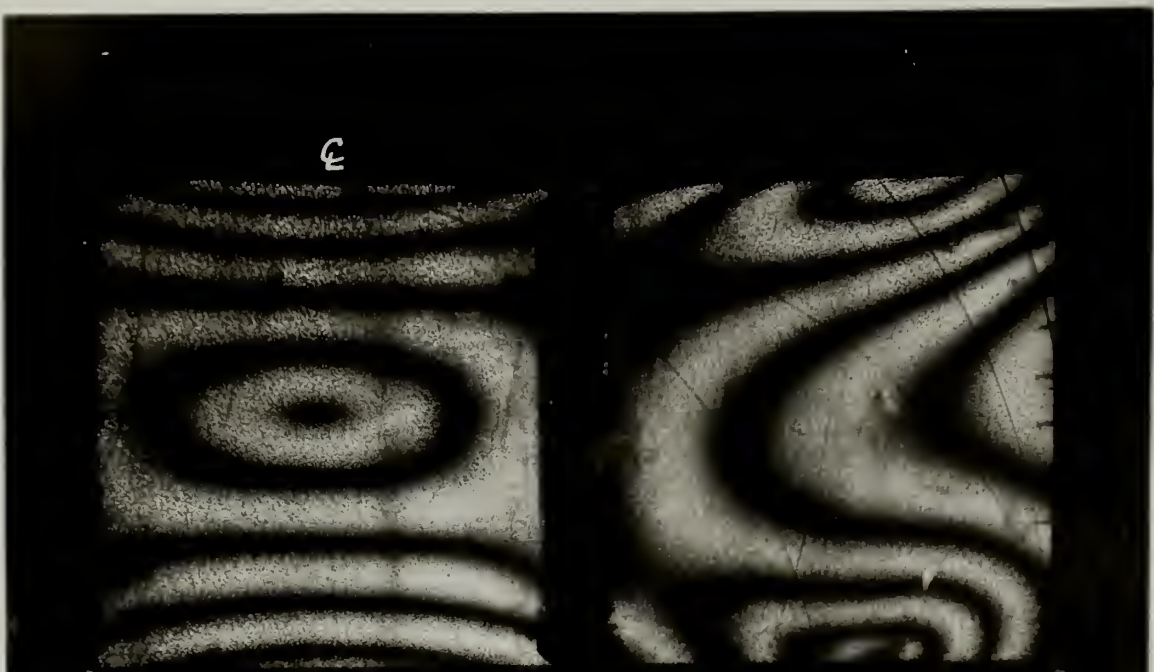

BOTTOM SUPPORTED

TABLE X

Aspect Ratio 5:1 — 2 Stiffeners

Load 300 psi.

Bottom Unsupported

Station	Order	θ	2θ	Sin 2θ	τ_{xy}	τ_{xy}/τ_m
0	5.8	0°	0°	0	0.0	0.0
1	5.9	16°	32°	.52992	538	.752
2	6.0	29°	58°	.84805	878	1.23
3	6.1	38°	76°	.97030	1020	1.43
4	6.4	47°	94°	.99756	1100	1.54
5	6.5	55°	110°	.93969	1050	1.47
6	6.4	62°	124°	.82904	915	1.28
7	6.2	69°	138°	.66913	715	1.00
8	6.1	76°	152°	.46947	494	.691
9	6.1	83°	166	.24193	254	.355
10	6.3	90°	180°	0	0.0	0.0

Bottom Supported

Station	Order	θ	2θ	Sin 2θ	τ_{xy}	τ_{xy}/τ_m
0	1.6	0°	0°	0	0	0.0
1	2.4	16°	32°	.52992	219.5	.307
2	3.0	27°	54°	.80902	418.9	.586
3	3.4	37°	74°	.96126	564.1	.79
4	3.6	45°	90°	1.00	621.36	.87
5	3.7	53°	106°	.97437	622.25	.87
6	3.5	61°	122°	.84805	512.0	.716
7	3.2	69°	138°	.66913	369.5	.517
8	2.8	76°	152°	.46947	226.88	.318
9	2.4	83°	166°	.24192	100.2	.14
10	2.1	90°	180°	0	0	0.0

Figure XLV

Sketch of Isoclinics and Data for AR 5:1
2 stiffeners and unsupported

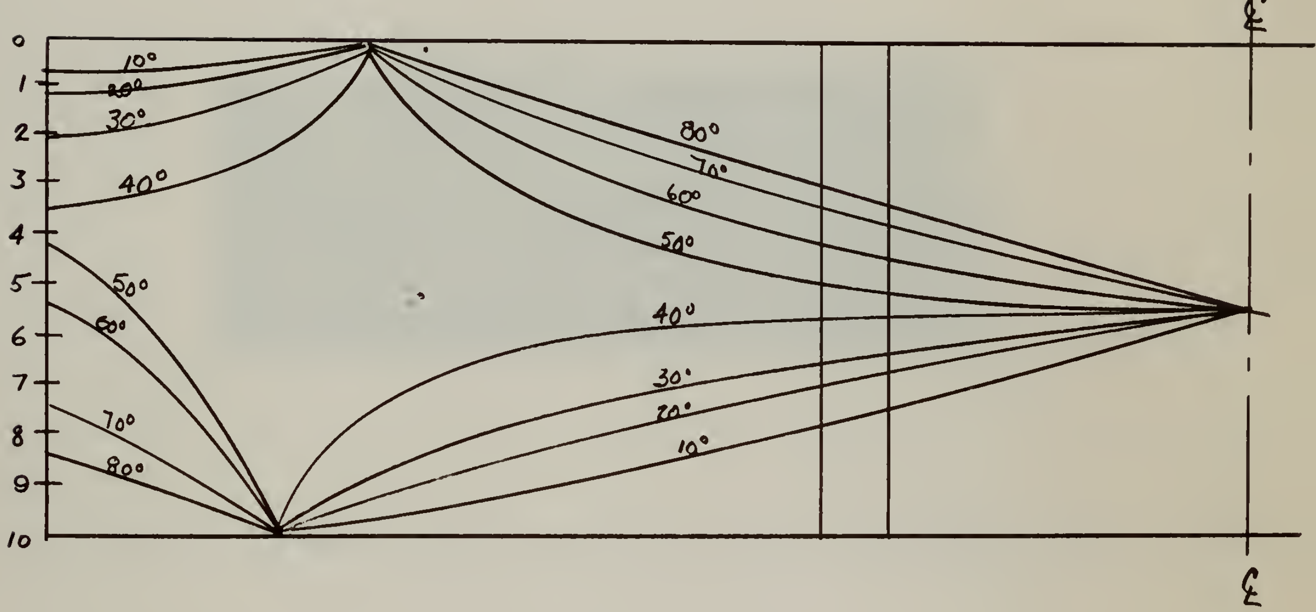

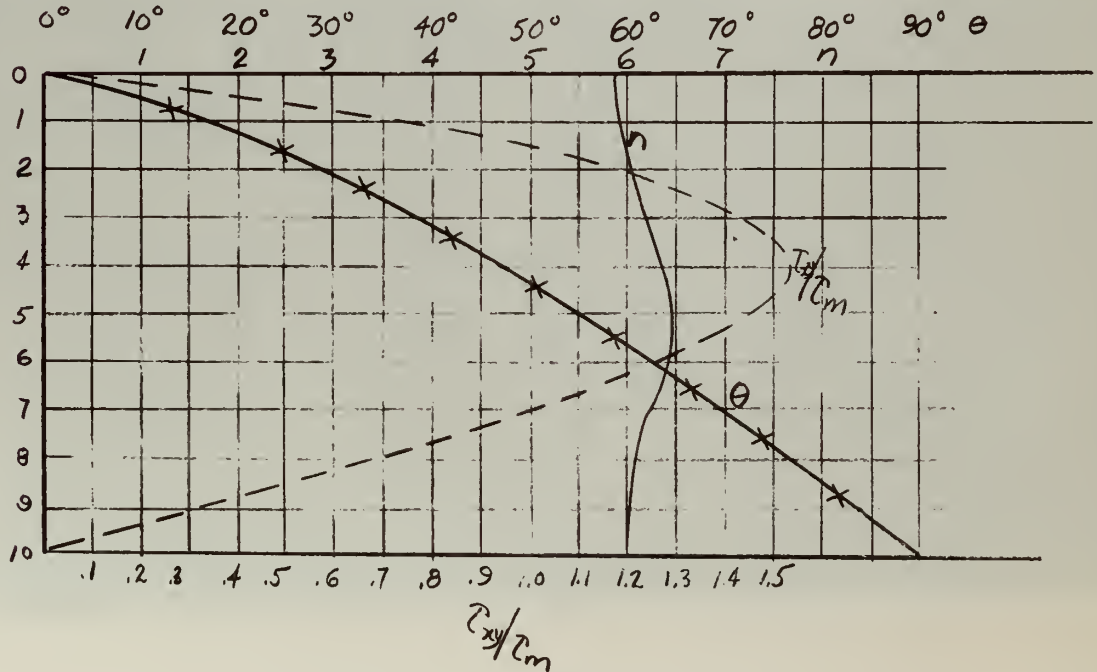

Figure XLVI

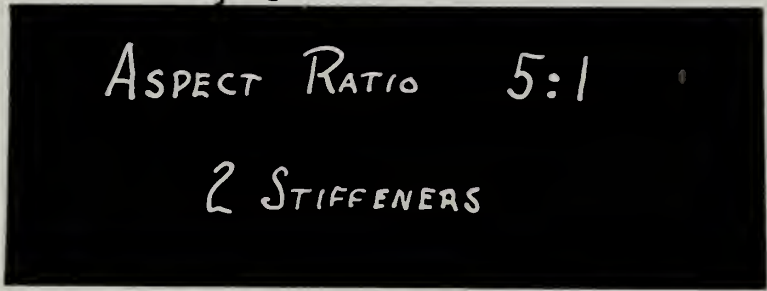

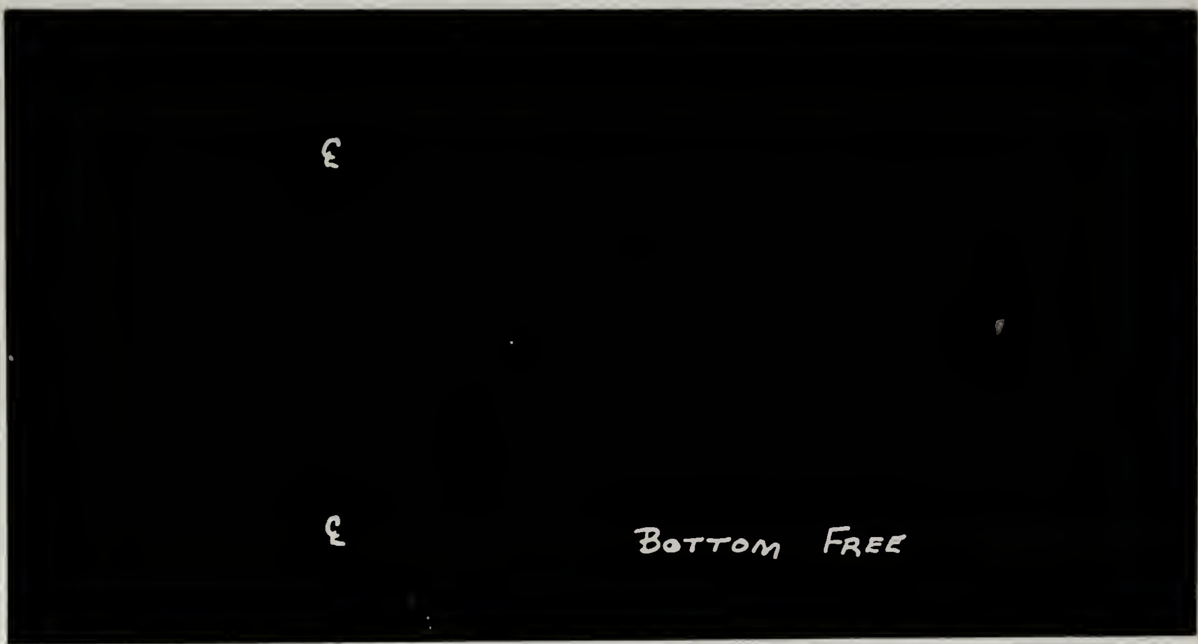

Figure XLVII

Sketch of Isoclinics and Data for AR 5:1
2 stiffeners and supported

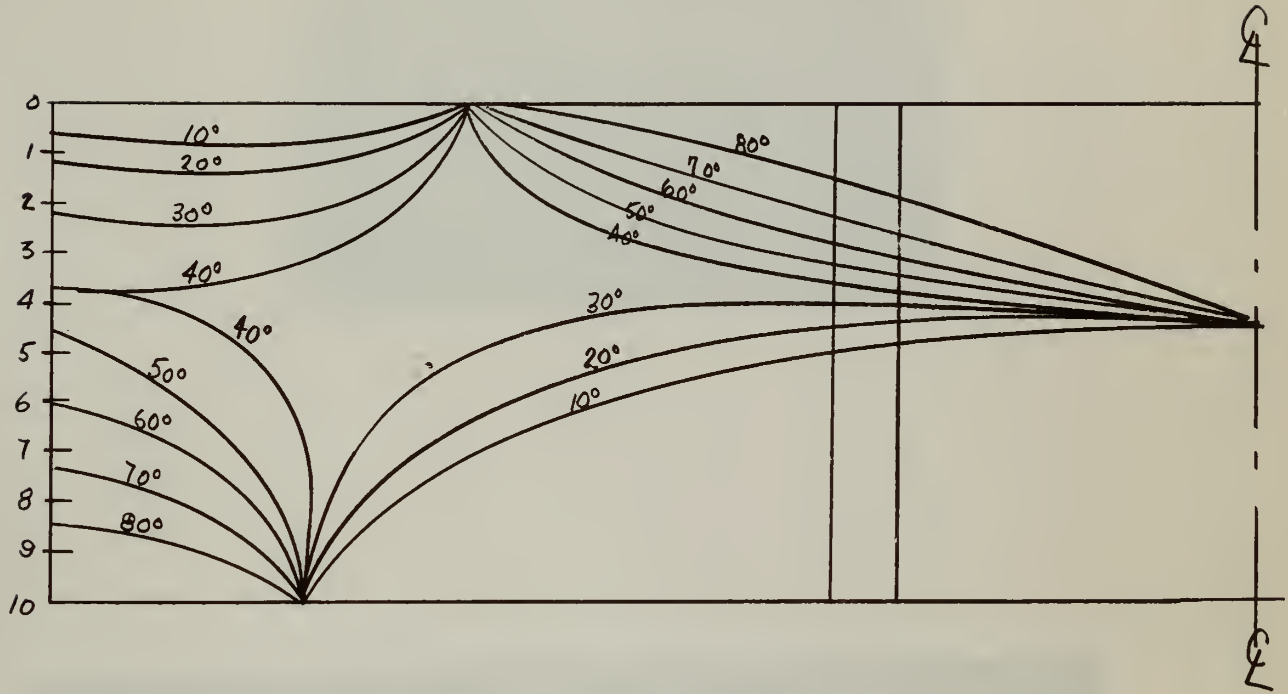

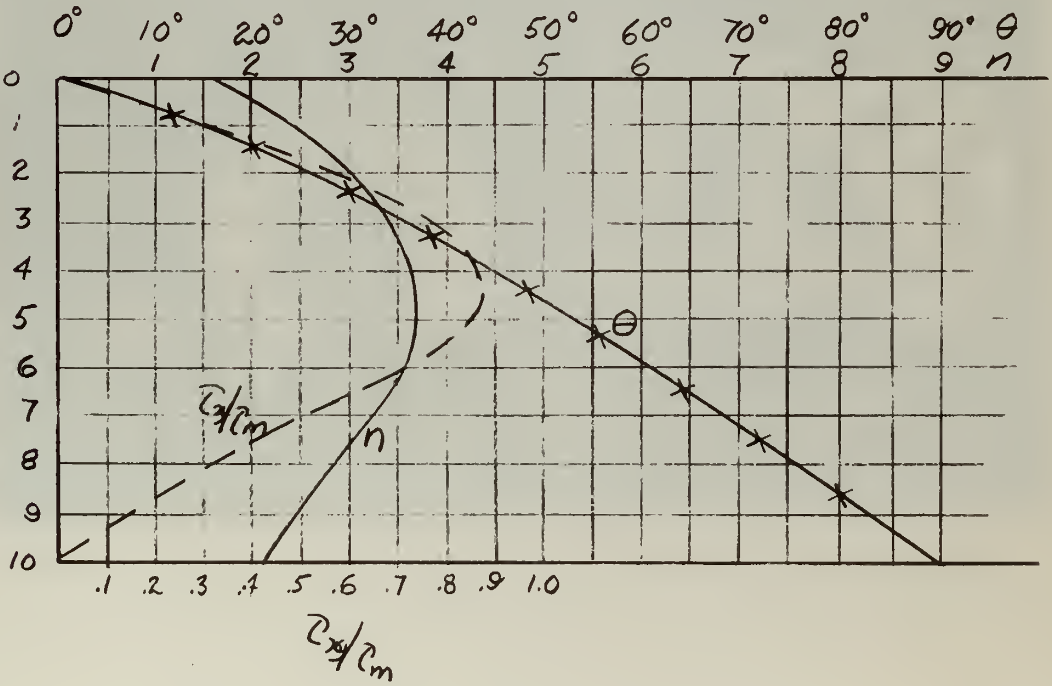

Figure XLVIII

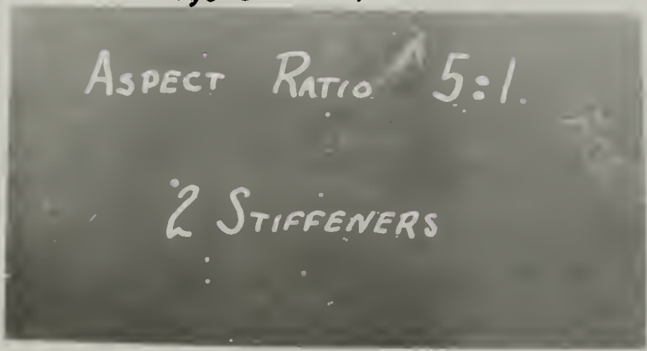

TABLE XI

Aspect Ratio 5:1 — 3 Stiffeners

Load 300 psi.

Bottom Unsupported

Station	Order	θ	2θ	Sin 2θ	τ_{xy}	τ_{xy}/τ_m
0	4.5	0°	0°	0	0.0	0.0
1	5.4	11°	22°	.37461	348.9	.488
2	6.0	18°	36°	.58779	608.7	.851
3	6.2	23°	46°	.71934	769.78	1.078
4	6.2	29°	58°	.84805	907.51	1.27
5	6.0	35°	70°	.93969	973.14	1.361
6	5.4	42°	84°	.99452	926.9	1.295
7	4.6	49°	98°	.99027	786.23	1.10
8	4.1	59°	118°	.88295	624.83	.874
9	4.0	75°	150°	.5000	345.2	.483
10	4.2	90°	180°	0	0.0	0.0

Bottom Supported

Station	Order	θ	2θ	Sin 2θ	τ_{xy}	τ_{xy}/τ_m
0	3.5	0°	0°	0	0.0	0.0
1	4.6	9°	18°	.30902	245.34	.343
2	5.0	19°	38°	.61566	531.3	.744
3	5.2	28°	56°	.82904	744.08	1.04
4	5.2	37°	74°	.96126	862.75	1.21
5	5.0	45°	90°	1.0	863.0	1.21
6	4.6	51°	102°	.97815	776.6	1.09
7	4.1	58°	116°	.89879	636.37	.89
8	3.8	65°	130°	.76604	502.43	.705
9	3.7	74°	148°	.52992	338.41	.474
10	3.4	90°	180°	0	0.0	0.0

Figure XLIX

Sketch of Isoclinics and Data for AR 5:1
3 stiffeners and unsupported

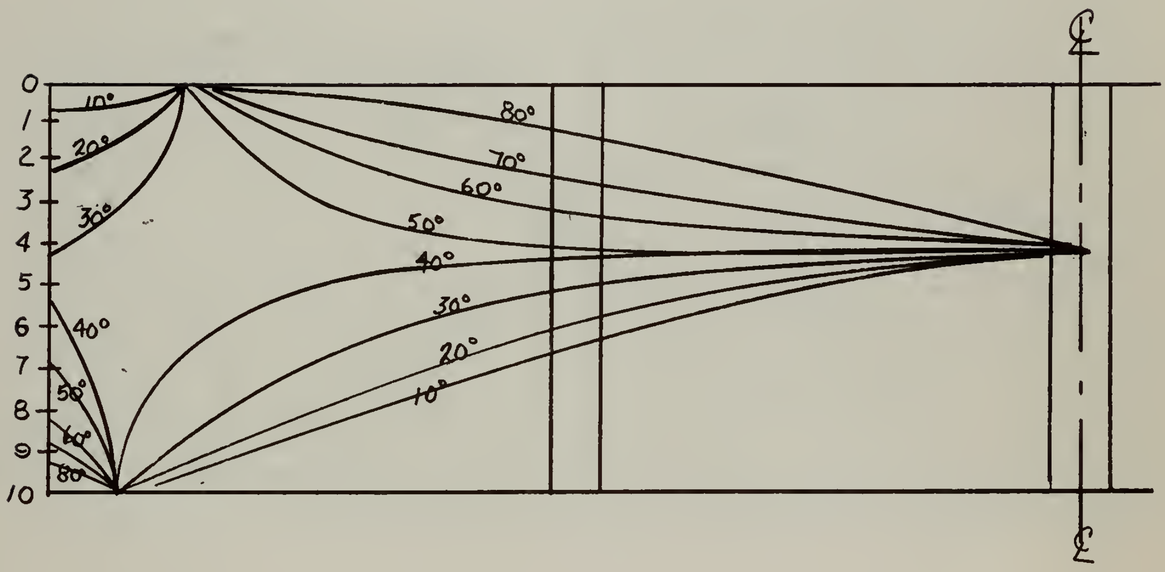

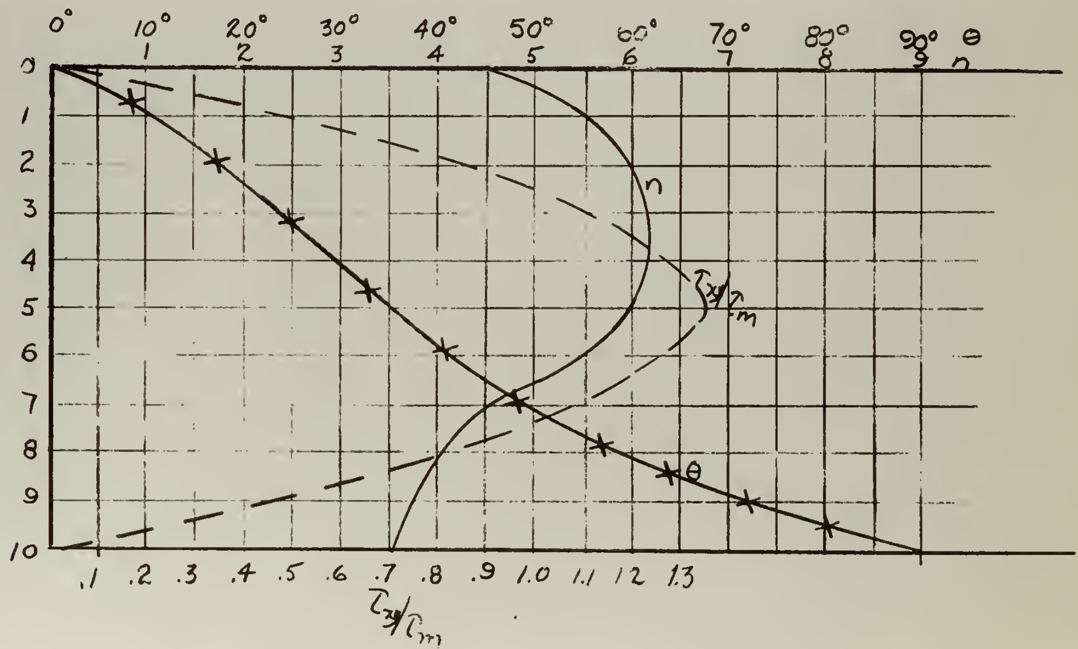

Figure XLX

Sketch of Isoclinics and Data for AR 5:1
3 stiffeners and supported

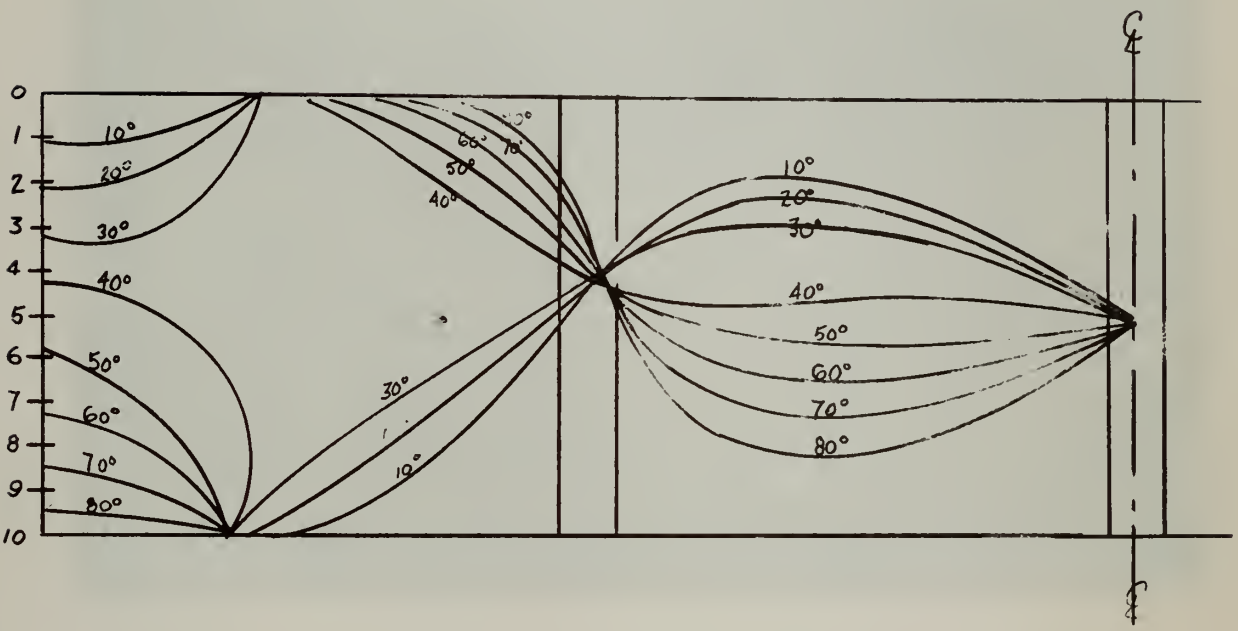

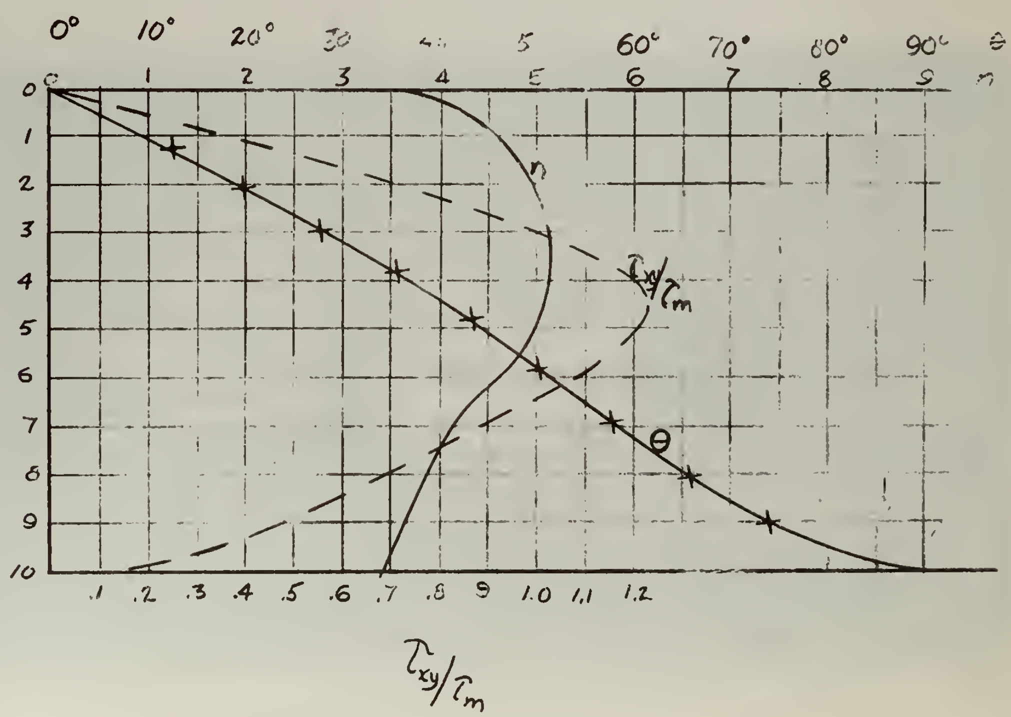

Figure XLXI

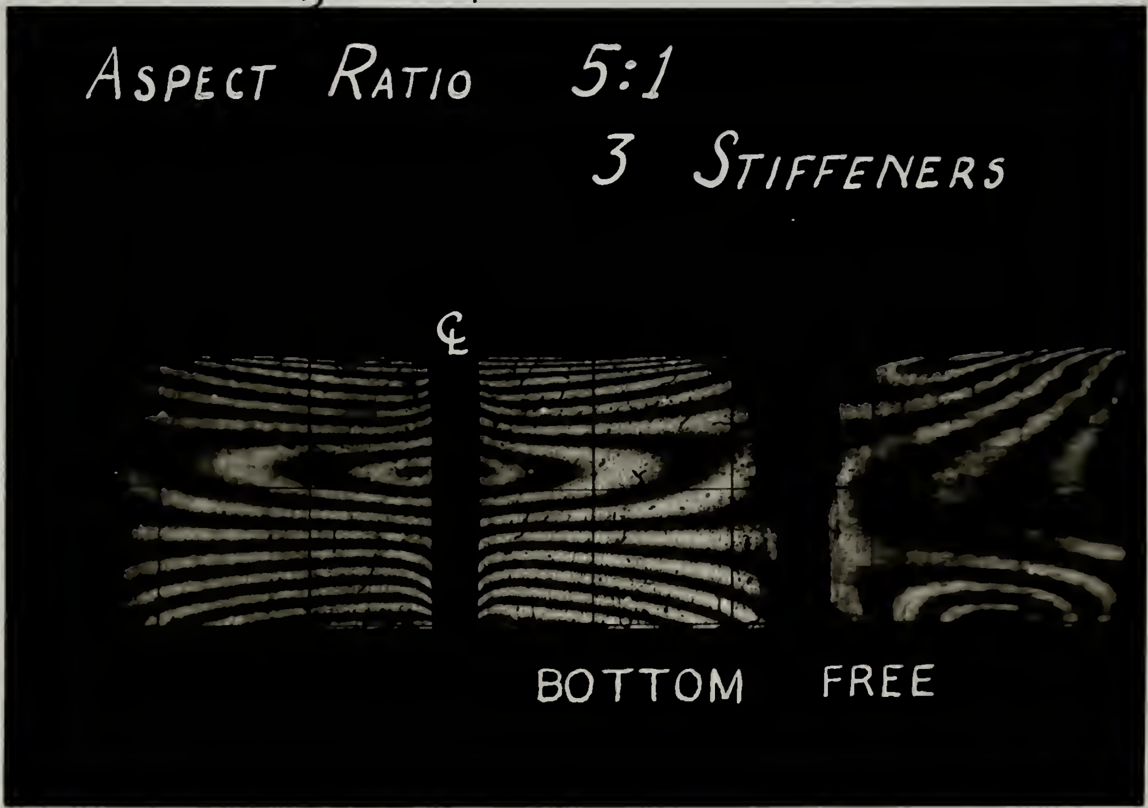

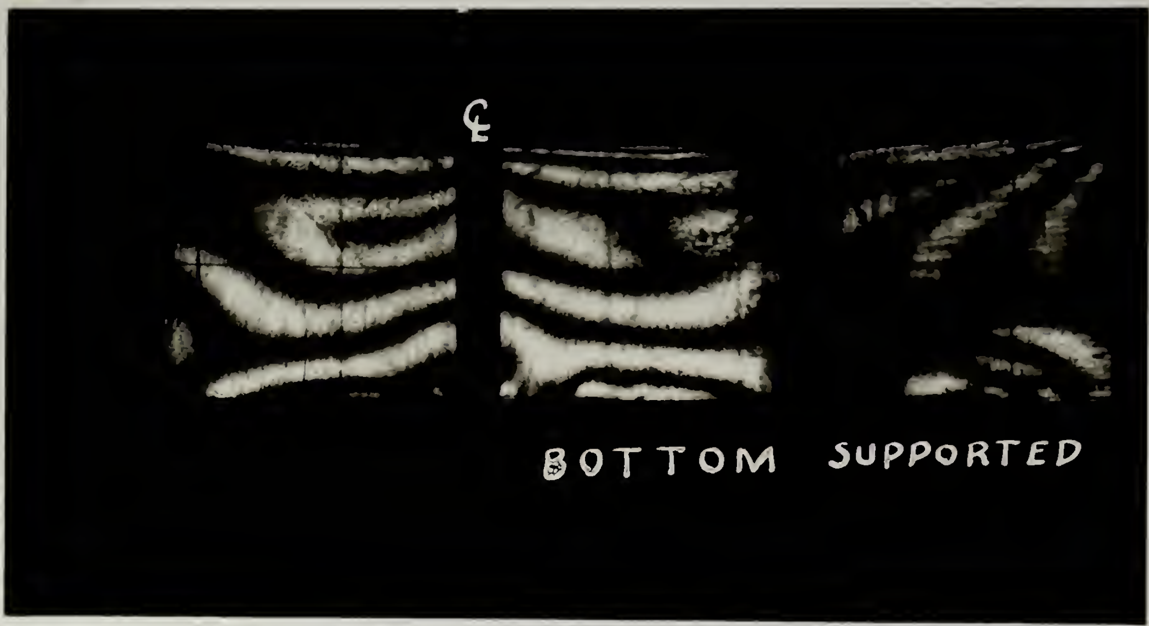

VIII REFERENCES

(1) Miller, E. A., Metcalf, J. T. "A Photoelastic Study of the Stress Distribution in Flat Plate Panels Simulating Ship Bulkheads" Thesis-Dept. of Naval Arch. and Marine Eng., M.I.T., 1957.

(2) Holman, R. "A Photoelastic Study of the Stress Distribution in Stiffened Plating" Thesis-Dept. of Naval Arch. and Marine Eng., M.I.T., 1956.

(3) Figueiredo, A. R., Marangiello, D. A., and Guerra, W. V. "A Photoelastic Study of the Stress Distribution in Ship Transverse Bulkhead" Thesis-Dept. of Naval Arch. and Marine Eng., M.I.T., 1956.

(4) Freire, T. D., DaSilva Sa, R. O., and Serrao, J.B.W. "A Photoelastic Study of the Stress Distribution in Flat Plating Panels" Thesis- Dept. of Naval. Arch. and Marine Eng., M.I.T., 1956.

(5) Frocht, M. M. "Photo-Elasticity", Vol. I, New York: John Wiley and Sons, 1941.

(6) Frocht, M. M. "Photo-Elasticity", Vol. II New York, John Wiley and Sons, 1948.

(7) Hetenyi, M. "Handbook of Experimental Stress Analysis", New York, John Wiley and Sons, 1950.

(8) Coker, E. G., and Filon, L.N.G. "Treatise on Photo-elasticity", Cambridge University Press, 1931

(9) Murray, W. M. "Class Notes on Experimental Stress Analysis" Course 2.126 M.I.T. 1957

(10) Timoshenko, S. and Goodier, J. N. "Theory of Elasticity" McGraw-Hill New York, 1951

(11) Gray, R. M., Lawton C. W. and Stitz, E. O. "Photoelasticity" Manual on Experimental Stress Analysis Techniques, Society for Experimental Stress Analysis, Cambridge, Mass., 1956.